JOURNAL OF PETROLOGY | VOLUME 45 | NUMBER 7 | PAGES 1339–1368 | 2004 | DOI: 10.1093/petrology/egh021

Partial Melting of Spinel Lherzolite in the System $CaO–MgO–Al_2O_3–SiO_2 \pm K_2O$ at 1·1 GPa

XI LIU* AND HUGH ST. C. O'NEILL†

RESEARCH SCHOOL OF EARTH SCIENCES, AUSTRALIAN NATIONAL UNIVERSITY, CANBERRA, A.C.T. 0200, AUSTRALIA

RECEIVED MAY 7, 2003; ACCEPTED JANUARY 22, 2004

The compositions of multiply saturated partial melts are valuable for the thermodynamic information that they contain, but are difficult to determine experimentally because they exist only over a narrow temperature range at a given pressure. Here we try a new approach for determining the composition of the partial melt in equilibrium with olivine, orthopyroxene, clinopyroxene and spinel (Ol + Opx + Cpx + Sp + Melt) in the system CaO–MgO–Al_2O_3–SiO_2 (CMAS) at 1·1 GPa: various amounts of K_2O are added to the system, and the resulting melt compositions and temperature are extrapolated to zero K_2O. The 'sandwich' experimental method was used to minimize problems caused by quench modification, and Opx and Cpx were previously synthesized at conditions near those of the melting experiments to ensure they had appropriate compositions. Results were then checked by reversal crystallization experiments. The results are in good agreement with previous work, and establish the anhydrous solidus in CMAS to be at 1320 ± 10°C at 1·1 GPa. The effect of K_2O is to depress the solidus by 5·8°C/wt %, while the melt composition becomes increasingly enriched in SiO_2, being quartz-normative above 4 wt % K_2O. Compared with Na_2O, K_2O has a stronger effect in depressing the solidus and modifying melt compositions. The isobaric invariant point in the system CMAS–K_2O at which Ol + Opx + Cpx + Sp + Melt is joined by sanidine (San) is at 1240 ± 10°C. During the course of the study several other isobaric invariant points were identified and their crystal and melt compositions determined in unreversed experiments: Opx + Cpx + Sp + An + Melt in the system CMAS at 1315 ± 10°C; in CMAS–K_2O, Opx + Cpx + Sp + An + San + Melt at 1230 ± 10°C and Opx + Sp + An + San + Sapph + Melt at 1230 ± 10°C, where An is anorthite and Sapph is sapphirine. Coexisting San plus An in three experiments help define the An–San solvus at 1230–1250°C.

KEY WORDS: *feldspar solvus; igneous sapphirine; mantle solidus; partial melting; systems CMAS and CMAS–K_2O*

INTRODUCTION

The simplest chemical system that contains all the major phases of peridotitic upper mantle (olivine, orthopyroxene, clinopyroxene, and an aluminous phase, one of plagioclase, spinel or garnet, depending on pressure) is $CaO–MgO–Al_2O_3–SiO_2$ (CMAS). This simple system has been used to investigate the basic phase relations of partial melting in the upper mantle (O'Hara, 1968; Kushiro, 1972; Presnall *et al.*, 1979; Longhi, 1987; Gudfinnsson & Presnall, 1996; Herzberg & Zhang, 1998; Milholland & Presnall, 1998; Presnall, 1999; Liu & Presnall, 2000). However, with a typical four-phase lherzolite assemblage, the initial melting in CMAS is isobarically invariant; that is, the chemical potentials of all four components (CaO, MgO, Al_2O_3 and SiO_2) in the melt are completely defined, as in

$$\underset{\text{Melt}}{CaO} + 1{\cdot}5\ \underset{\text{Opx}}{Mg_2Si_2O_6} = \underset{\text{Cpx}}{CaMgSi_2O_6} + \underset{\text{Ol}}{Mg_2SiO_4} \quad (1)$$

$$\underset{\text{Melt}}{MgO} + 0{\cdot}5\ \underset{\text{Opx}}{Mg_2Si_2O_6} = \underset{\text{Ol}}{Mg_2SiO_4} \quad (2)$$

$$\underset{\text{Melt}}{SiO_2} + \underset{\text{Ol}}{Mg_2SiO_4} = \underset{\text{Opx}}{Mg_2Si_2O_6} \quad (3)$$

*Present address: Geodynamics Research Center, Ehime University, Matsuyama 790-8577, Japan.
†Corresponding author. Telephone: (61) 2 6125 5159. Fax: (61) 2 6125 5989. E-mail: hugh.oneill@anu.edu.au

and, in the Sp-lherzolite stability field,

$$\underset{\text{Melt}}{Al_2O_3} + \underset{\text{Ol}}{Mg_2SiO_4} = \underset{\text{Sp}}{MgAl_2O_4} + 0{\cdot}5\ \underset{\text{Opx}}{Mg_2Si_2O_6}. \quad (4)$$

Because all chemical potentials are known, the composition of the melt in equilibrium with all four solid phases is particularly valuable in constructing thermodynamic models of silicate melts. Unfortunately, the isobarically invariant melt composition is difficult to determine experimentally, because the five-phase assemblage exists only over an infinitely narrow temperature interval at a given pressure.

The traditional way around this problem is to bracket the isobaric invariant point by varying the experimental starting composition, to produce four-phase isobarically univariant assemblages (i.e. three solid phases plus melt as in Fo + Opx + Sp + Melt). Not only does this require a large number of experiments, but it is tedious to demonstrate equilibrium (Presnall *et al.*, 1978; Liu & Presnall, 1990), as the solid phases (especially the pyroxenes) are multicomponent solid solutions with the potential to be compositionally unequilibrated. This method also requires some extrapolation to the isobaric invariant point, as this point is only bracketed.

Alternatively, it is possible to rely on experimental imperfections, such as temperature gradients or chemical impurities (e.g. some Na_2O in the starting material or H_2 diffusing through the Pt capsule to produce H_2O in the experimental charge) to increase the effective variance of the system and obtain melt in equilibrium or quasi-equilibrium with four solid phases, which can then be analysed directly. This approach has been adopted by Presnall and colleagues (Presnall *et al.*, 1979; Gudfinnsson & Presnall, 1996; Milholland & Presnall, 1998; Liu & Presnall, 2000). Although this seems empirically to work well for the system CMAS, this may not always be the case, and we have encountered insuperable difficulties in applying this approach to determining the effect of Cr_2O_3 on melting in the system CMAS–Cr_2O_3. Relying on semi-controlled imperfections to obtain a result is also intellectually unsatisfying, and the question arises of how much the imperfections affect results.

In this paper we report a logical improvement to this approach, which is to introduce another component into the system deliberately. The system is then studied as a function of the controlled concentration of this component, such that the composition of the CMAS isobaric invariant melt can be obtained by extrapolating to zero concentration of the added component. We chose K_2O as the additional component (the K_2O-method hereafter), as it is almost completely incompatible in all the solid phases (Ol, Opx, Cpx, Sp) at our chosen experimental pressure of 1·1 GPa. Having the extra component entering only the melt phase makes the extrapolation to the pure CMAS system simple. Also, K_2O is an important constituent in several mantle-derived magma types (kimberlites, shoshonites, and so on), so that our data for the system CMAS–K_2O generated as a by-product of our main purpose should be of some direct petrological relevance.

We show that the K_2O-method produces a result in good agreement with the previous work of Presnall and colleagues (Presnall, 1976; Presnall *et al.*, 1979; Walter & Presnall, 1994), and our improved accuracy allows for some refinement of this work.

EXPERIMENTAL AND ANALYTICAL TECHNIQUES

Four types of experiments were performed:

(1) conventional direct partial melting experiments (DEs) in the system CMAS;

(2) sandwich experiments using the K_2O-method (KEs), in which the solid assemblage Fo + Opx + Cpx + Sp was placed at the top and bottom of the capsule, with a K_2O-containing melt composition as the 'filling';

(3) reversal experiments (REs-1) to study the crystallization of the CMAS melt composition deduced from the KEs;

(4) reversal experiments (REs-2) with Fo added; all but one of these (C-1789) used the sandwich configuration.

Starting materials

Table 1 summarizes the starting materials used in this study. Compositions were made from high-purity oxides (SiO_2, Al_2O_3 and MgO) and carbonates ($CaCO_3$ and K_2CO_3). An important strategy was to use pre-synthesized Opx and Cpx with compositions similar to those expected in the run products.

Mix9 was prepared by combining a crystalline mixture of pure forsterite (Fo) and a crystalline mixture of Sp + Opx + Cpx in a proportion of 1:5 by weight. The Fo was synthesized at 1400°C and atmospheric pressure for 69 h; the mixture with Sp:Opx:Cpx in weight proportions of 1:2:2 was made in a 5/8 inch piston-cylinder press using a 3·5 mm diameter Pt capsule and a talc–Pyrex assembly at 1280°C and 1·1 GPa for 48 h. The phase proportion in the final Mix9 was close to 1:1:2:2 (Fo:Sp:Opx:Cpx). Crystalline mixture SEM02-1 containing Fo:Sp:Opx:Cpx = 1:1:1:1 (by weight) was made by crystallizing the decarbonated oxide mix at 1300°C and 1·1 GPa for 48 h in a Pt capsule. Mixtures SEM02-3, SEM02-4, SEM02-8 and SEM02-6 were melted at 1400°C and 1 atm for 20 min and then quenched to glass.

All mixtures were checked for compositions with electron microprobe (Ware, 1991). Mix9 was later stored in

Table 1: Starting compositions used in this study

	Mix9 cryst.	SEM02-1 cryst.	SEM02-3 glass	SEM02-4 glass	SEM02-10 glass	SEM02-8 glass	SEM02-6 glass	SEM02-13 glass
SiO_2	42·12	36·95	48·71	49·37	57·69	59·33	49·09	57·13
Al_2O_3	18·34	22·63	18·97	20·20	20·80	23·13	20·12	17·89
MgO	32·46	35·06	16·60	13·52	6·20	2·57	15·45	11·72
CaO	7·08	5·36	14·72	13·91	6·81	4·99	15·33	4·48
K_2O	0·00	0·00	1·00	3·00	8·49	10·00	0·00	8·79

Mix9 contains Fo:Sp:Opx:Cpx in the proportion 1:1:2:2 where Fo is forsterite, Sp spinel, Opx orthopyroxene and Cpx clinopyroxene. Fo was synthesized at 1400°C, 1 bar for 69 h, whereas Sp + Opx + Cpx were synthesized together at 1280°C, 1·1 GPa for 48 h. SEM02-1 contains Fo:Sp:Opx:Cpx in the proportion of 1:1:1:1, made up as for Mix9. SEM02-3 and SEM02-4 from 116-3 (Walter & Presnall, 1994), first normalized to 99 or 97 wt % and then 1 or 3 wt % K_2O added, respectively. SEM02-10 is the melt composition from C-1585. SEM02-8 is the melt composition from earlier KEs extrapolated to 10 wt % K_2O (See Fig. 4) However, it was found to contain more Al_2O_3 than that in the equilibrium melt, crystallizing sapphirine (see text for details). SEM02-6 is the melt composition from the KEs extrapolated to 0 wt % K_2O (See Fig. 3), used as the starting material in the REs. SEM02-13 contains 80% melt + 5% San + 15% Fo in which the composition of melt and San (Sanidine) is from C-1708.

an oven at 110°C and other starting materials were stored in another oven at 150°C.

Piston-cylinder assemblies

All experiments were made in a conventional half-inch piston-cylinder apparatus (Boyd & England, 1960). The salt–Pyrex pressure assembly used in the preliminary DEs was described by Klemme & O'Neill (1997), except that, because of the generally lower pressure and temperature regime of this study, fired pyrophyllite replaced the MgO spacer underneath the capsule and mullite was used instead of high-purity alumina for the thermocouple tube. Further modification for the assembly used in the KEs and the REs were made because of possible H_2 diffusion into the Pt capsule causing contamination of the runs by H_2O. In these experiments the Pt capsule was held in an Fe_2O_3 sleeve, which was in turn surrounded by an alumina sleeve. At each end of the alumina sleeve, a ruby disc (0·5 mm thick) separated the Fe_2O_3 sleeve from other parts of the assembly. This structure prevents the Fe_2O_3 sleeve from being reduced by the graphite heater, or contaminating the thermocouple. Alumina spacers and then MgO spacers were positioned next to both ruby discs, to enhance the mechanical stability of the assembly. The thermocouple was protected by a combination of high-purity alumina tubing in the hot part of the assembly (~4 mm long), followed by mullite tubing above this. The Fe_2O_3 sleeve was made by cold pressing in a steel die and then sintered at atmospheric pressure and 850°C for 3 h, using acetone as a binder.

These salt–Pyrex assemblies have low friction and no pressure correction is required, considering the high temperatures and long run times used in this study (Green *et al.*, 1966; Bose & Ganguly, 1995; Klemme & O'Neill, 1997).

Experimental procedures

For each experiment, 8–10 mg starting materials were loaded into a Pt capsule. The capsules used in the DEs were stored at 110°C for 6–8 h before welding. The Pt capsules for the KEs and REs were stored at 150°C for 6–8 h, then held in a steel block that had been pre-heated to 750°C while they were welded (Robinson *et al.*, 1998).

All experiments were performed using the 'piston-out' method, i.e. the pressure was first raised to several MPa, then the temperature was raised to *c.* 450°C to soften the Pyrex sleeve. The pressure was then increased to *c.* 0·05 GPa higher than the desired pressure, the temperature was raised to the nominal temperature of the run, and finally the pressure was lowered to the required pressure (Johannes *et al.*, 1971). Pressures were continuously monitored and adjusted, if necessary, which allowed each run to be controlled within ±0·02 GPa of the nominal pressure. Temperature was measured and controlled with $Pt_{94}Rh_6$–$Pt_{70}Rh_{30}$ thermocouple (type B), previously calibrated against the melting point of gold at atmospheric pressure; possible pressure effects on the e.m.f. of the thermocouple were neglected. The tip of the thermocouple, the upper ruby disc and the whole Pt capsule containing the experimental charge were all carefully placed in the 5-mm-long hot spot of the experimental assembly. Although temperature during experiments was controlled to ±1°C, the true temperature uncertainties are estimated to be *c.* ±5–10°C, mainly because of slight differences in sample position and power density through the graphite heater. Such an uncertainty is consistent with the variations in melt composition and other experimental parameters observed in these experiments. A discussion of the superior merits of type B thermocouples over other Pt/Rh thermocouples or W/Re thermocouples at temperatures near 1300°C has been given by Klemme & O'Neill (2000*b*).

Table 2: Comparison of electron microprobe analyses and recommended values for secondary standards

	GOR132G		KL2G		T1G	
	71*	Rec. V.	57	Rec. V.	56	Rec. V.
SiO_2	46·08(0·26)*	45·98(0·30)	51·33(0·20)	51·37(0·10)	59·56(0·22)	59·28(0·20)
TiO_2	0·32(0·08)	0·29(0·01)	2·70(0·09)	2·67(0·05)	0·77(0·07)	0·74(0·01)
Al_2O_3	11·10(0·22)	11·02(0·10)	13·51(0·11)	13·43(0·10)	17·17(0·12)	17·23(0·10)
Cr_2O_3	0·38(0·08)	0·36(0·01)	0·05(0·07)	0·05(0·00)	0·04(0·05)	0·00(0·00)
FeO	10·21(0·20)	10·21(0·10)	10·78(0·22)	10·97(0·10)	6·49(0·16)	6·51(0·04)
MnO	0·17(0·08)	0·15(0·00)	0·18(0·10)	0·17(0·00)	0·11(0·07)	0·13(0·00)
MgO	22·17(0·27)	22·64(0·10)	7·37(0·07)	7·44(0·06)	3·71(0·07)	3·79(0·04)
CaO	8·57(0·13)	8·51(0·09)	11·19(0·13)	11·07(0·10)	7·13(0·10)	7·17(0·05)
Na_2O	0·98(0·06)	0·81(0·01)	2·42(0·08)	2·33(0·04)	3·06(0·13)	3·18(0·03)
K_2O	0·03(0·04)	0·03(0·00)	0·46(0·05)	0·49(0·01)	1·96(0·06)	1·97(0·02)

71*: the number of electron microprobe analyses. 46·08(0·26) should be read as 46·08 ± 0·26. Analysis was normalized to 100 wt % before the average and the standard deviation were calculated. For the recommended values, Rec. V., normalized results to 100 wt % are used to facilitate comparison. The standard deviation of the recommended values, however, is directly from Jochum *et al*. (2000).

Analytical methods

At the end of a run, the sample was sectioned longitudinally, mounted in epoxy and polished using a series of diamond pastes. Run products were carbon-coated and analysed on a Cameca electron microprobe at the Research School of Earth Sciences (RSES), ANU and/or on a JEOL 6400 scanning electron microprobe in energy dispersive mode (EDS) at the Electron Microprobe Unit (EMU) at ANU. Coexisting phases in all run products were identified by back-scattered electron imaging. Beam current was 1 nA, accelerating voltage was 15 keV and ZAF correction was applied in all analyses (Ware, 1991). A beam spot size of 1 μm was used for all crystalline phases, and both 1 μm and 10 μm beam spot sizes were used for glass analyses. Calibration was based on optimization to a large number of standards; to check this calibration and also as a monitor of any drift between analysing sessions, we repeatedly analysed three glass standards, GOR132G, T1G, and KL2G, which have comparable compositions to the phases present in this study (Jochum *et al*., 2000). The 185 analyses over 24 analytical sessions are summarized in Table 2. There is excellent agreement between our electron probe analyses and the recommended values.

Besides the major oxides CaO, MgO, Al_2O_3, SiO_2, and K_2O expected in the run products, we also routinely analysed for FeO, Cr_2O_3, and Na_2O in all phases. Either diffusion of Fe through the Pt capsule from the Fe_2O_3 sleeve or a leak in the capsule could result in Fe contamination. Na_2O appears to be a good indicator of the purity of the starting materials. It concentrates in the melt, and 0·1–0·3 wt % was found in the glasses in this study, depending on the proportion of melt to solid in the experiment. Such a concentration is close to the limit of detection by EDS, and has been ignored as it has a minimal effect on the phase relations (Walter & Presnall, 1994; Liu *et al*., in preparation).

Lithium and boron have potentially been cryptic contaminants of previous piston-cylinder studies, as only recently have these elements become amenable to microbeam analysis. Li salts are sometimes used in noble-metal fabrication processes, and B could come from the Pyrex glass (it apparently diffuses readily through Pt). To check for any such contamination, Li and B were measured in the glasses in runs C-1422, C-1448 and C-1565 (see Table 3 for experimental conditions) by laser ablation–inductively coupled plasma–mass spectrometry at RSES, ANU. The Li contents were 4·1 ± 0·2 ppm, 4·1 ± 0·1 ppm and 2·8 ± 0·4 ppm, respectively. The B contents were slightly higher at 53 ± 2, 54 ± 2 and 52·3 ± 7 ppm. We assume these levels have a negligible effect on phase relations.

Fe_2O_3 sleeve and H_2O contamination

Following Robinson *et al*. (1998), Fe_2O_3 sleeves were used as H_2-getters surrounding the Pt capsule in all experiments apart from the first few reported in this study (the DEs). The idea is that an oxidized substance such as Fe_2O_3 should react with H_2, which may be produced in the piston-cylinder assembly by contaminant moisture reacting with the graphite heater, for example. The getter should minimize the ingress of H_2 into the Pt capsule by diffusion, where it can react with silicates (e.g. alloying

Table 3: Experimental conditions and phase assemblages

Run no.	Starting material	Fe_2O_3	ST	*T* (°C)	Time (h)	Phase assemblage	K_2O-melt	T-NBK85
DEs								
C-1111	Mix9	No	No	1330	48	Fo + Sp + Opx + Melt		
C-1556	Mix9	No	No	1310	56	Fo + Sp + Opx + Melt		
C-1555	Mix9	No	No	1300	56	Fo + Sp + Opx + Cpx + Melt(tr)		1316
KEs								
C-1417	SEM02-1 + SEM02-3	Yes	Yes	1330	60	Fo + Sp + Melt	0·59	
C-1423	SEM02-1 + SEM02-3	Yes	Yes	1320	55	Fo + Sp + Melt	0·63	
C-1422	SEM02-1 + SEM02-3	Yes	Yes	1310	55	Fo + Sp + Opx + Cpx + Melt	0·73	1337
C-1461	SEM02-1 + SEM02-4	Yes	Yes	1310	75	Fo + Sp + Opx + Cpx + Melt	2·31	1326
C-1448	SEM02-1 + SEM02-4	Yes	Yes	1300	70	Fo + Sp + Opx + Cpx + Melt	4·08	1331
C-1460	SEM02-1 + SEM02-4	Yes	Yes	1290	75	Fo + Sp + Opx + Cpx + Melt	4·76	1315
C-1447	SEM02-1 + SEM02-4	Yes	Yes	1280	70	Fo + Sp + Opx + Cpx + Melt	6·20	1332
C-1574	SEM02-1 + SEM02-8	Yes	Yes	1270	93	Fo + Sp + Opx + Cpx + Melt	8·35	1310
C-1585*	SEM02-1 + SEM02-8	Yes	Yes	1240/1260	72/123	Fo + Sp + Opx + Cpx + Melt	8·49	1300
C-1779	SEM02-1 + SEM02-13	Yes	Yes	1250	217	Sp + Opx + Cpx + San + Melt + Fo(?)	10·09	1251
C-1701	SEM02-1 + SEM02-10	Yes	Yes	1240	17	Sp + Opx + Cpx + An + Melt + Fo(?)	9·17	1295
C-1708	SEM02-1 + SEM02-10	Yes	Yes	1230	195	Sp + Opx + Cpx + An + San + Melt	10·12	1238
C-1580†	SEM02-1 + SEM02-8	Yes	Yes	1250	159	Fo + Sp + Opx + Cpx		
						An + San + Sapph + Melt	9·33	
C-1576†	SEM02-1 + SEM02-8	Yes	Yes	1230	98	Fo + Sp + Opx + Cpx		
						Sp + Opx + An + San + Sapph + Melt	8·98	
REs-1								
C-1621	SEM02-6	Yes	No	1340	24	Melt		
C-1639	SEM02-6	Yes	No	1320	54	Sp + Opx + Cpx + Melt		1337
C-1565	SEM02-6	Yes	No	1320	26	Sp + Opx + Cpx + An + Melt		1336
C-1566	SEM02-6	Yes	No	1310	48	Opx + Cpx + An + Melt(tr)		1318
REs-2								
C-1769	Fo + SEM02-6	Yes	Yes	1340	24	Fo + Melt		
C-1767	Fo + SEM02-6	Yes	Yes	1320	62	Fo + Opx + Melt		
C-1781	Fo + SEM02-6	Yes	Yes	1315	91	Fo + Sp + Opx + Cpx + Melt		1326
C-1768†	Fo + SEM02-6	Yes	Yes	1315	66	Fo + Sp + Opx + Cpx		1356
						Sp + Opx + Cpx + An		1321
C-1789	Fo + SEM02-6	Yes	No	1300	104	Fo + Sp + Opx + Cpx		1305

Fe_2O_3, Fe_2O_3 external sleeve was always used together with hot block-welding technique. ST, sandwich technique. T-NBK85, temperature (°C) calculated from the two-pyroxene thermometer for CMAS of Nickel *et al*. (1985). DEs, direct partial melting experiments in system CMAS; KEs, partial melting experiments using the K_2O-method; REs, reversal crystallization experiments. Fo, forsterite; Sp, spinel; Opx, orthopyroxene; Cpx, clinopyroxene; An, K_2O-bearing anorthite; San, sanidine; Sapph, sapphirine; tr, only trace amount present. Fo(?), residual Fo only.
*The temperature in this experiment was first held at 1240°C for 72 h and then adjusted to 1260°C for 123 h.
†Disequilibrium between the different layers of the sandwich.

some Si into the Pt in FeO-free systems), thus forming H_2O. According to Robinson *et al.* (1998), the use of Fe_2O_3 sleeves coupled with careful drying of capsules before and during welding can reduce the H_2O content in experimental melts from ~1 wt % to ~0·1 wt %.

The Fe_2O_3 sleeves after two experiments (C-1417 and C-1566; see Table 3 for experimental conditions) were checked by powder X-ray diffraction at the Geology Department, ANU and were found to be >99 wt % Fe_2O_3. This does not mean that the sleeves were unnecessary, however, as analysis of the Pt capsules (using the Cameca electron microprobe in wavelength-dispersive mode at RSES, ANU) showed an Fe diffusion gradient. An example is given in Fig. 1 (1340°C, 1·1 GPa, 72 h).

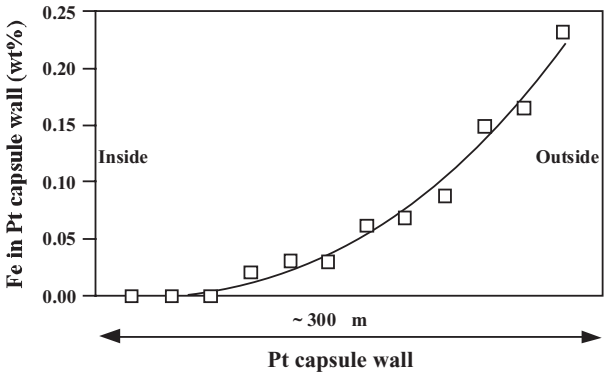

Fig. 1. Profile of Fe diffusion into a Pt capsule wall. Experimental conditions: 1·1 GPa, 1340°C, 72 h. Curve is fitted by eye.

Whereas Fe metal reached the middle point of the capsule wall, the experimental charge remained untouched. Longer run times or higher temperatures would result in Fe reaching the inner wall of the capsule, hence the need to analyse Fe routinely in run products.

C-1621 contains only melt (see Table 3 for experimental conditions) and is ideal for using transmission infrared spectroscopy to determine the water content. Details of this procedure as implemented in this study will be reported by Liu *et al.* (in preparation). The average water content from seven analyses is 120 ppm, which is substantially lower than the 0·1% reported by Robinson *et al.* (1998) and the 1100 ppm by Falloon *et al.* (1999); Baker *et al.* (1996) and Falloon *et al.* (2001) estimated an even larger amount, 0·5–1%, in their nominally anhydrous experiments. If the same total of H_2O as in run C-1621 were concentrated into the melt phase in those runs with smaller proportions of melt, the H_2O concentrations might be higher than in C-1621, but it seems unlikely that levels of H_2O in any run with the Fe_2O_3 sleeves would exceed 0·1%.

Attainment of equilibrium

There is a fundamental dilemma to be addressed in designing experiments aimed at obtaining the compositions of partial melts at modest degrees of melt fraction. To optimize equilibration between melt and crystals, it is obviously advantageous to have the melt distributed between crystals, to maximize mutual contacts. This is the usual texture formed in simple experiments (the DEs of this study) with less than about 20–30% melt, in the absence of a temperature gradient. However, maximizing the contact between melt and crystals also maximizes the probability of quench modification by precipitation on the rims of crystals. In addition, melt so distributed is difficult to analyse accurately, as melt pockets are small and irregularly shaped. This latter problem becomes worse as the melt fraction decreases. The experimental solution to these problems has been to devise ways of separating the melt from the crystals, as in sandwich experiments (as in this study and Stolper, 1980; Takahashi & Kushiro, 1983; Fujii & Scarfe, 1985; Falloon & Green, 1987, 1988; Robinson *et al.*, 1998) or by extraction into diamond aggregates or similar (Baker *et al.*, 1992; Johnson & Kushiro, 1992; Kushiro & Hirose, 1992; Hirose & Kawamoto, 1995; Hirose, 1997). Another possible tactic is to exploit the temperature gradient present in many high-pressure experiments, particularly in multi-anvil experiments, to separate melt towards the hot end of the capsule (Takahashi, 1986). However, the inevitable consequence of any separation is to impair the chances of attaining equilibrium between melt and crystals.

The problems that this can cause are well illustrated in this study by two experiments, C-1580 and C-1576 (Table 3; see Fig. 2a), in which the initial composition chosen for the 'filling' part of the sandwich turned out not to be in equilibrium with the Fo + Opx + Cpx + Sp assemblage at the ends of the sandwich (the 'bread'), despite the long run times used in these experiments. Instead, the run products consisted of three zones: (1) the initial Fo + Opx + Cpx + Sp assemblage, which in these two runs is unequilibrated with respect to the pyroxene compositions (particularly Opx; see Table 4); (2) the 'filling' part, comprising melt plus An + Sapph + San (C-1580) or, in the lower-temperature experiment (C-1576), melt plus An + Sapph + San + Sp + Opx, the latter of which has a very different composition from the Opx in the Fo + Opx + Cpx + Sp assemblage; (3) a narrow reaction zone of Opx, no more than 20 μm wide, between the two other zones (see below). These textures are shown in Fig. 2a; for comparison, the texture developed in a successfully equilibrated sandwich experiment is given in Fig. 2b. The conspicuous inability of the melts in the 'filling' to re-equilibrate with the solid Fo + Opx + Cpx + Sp assemblage in these two runs may be due to their high SiO_2, and hence high viscosity.

The large difference in the composition of Opx in the different zones of C-1576 is instructive. Because the composition of a solid solution phase depends on its chemical environment, it is unlikely to be the same in the two different parts of a sandwich experiment unless these parts are in equilibrium. We therefore paid particular attention in this study to analysing pyroxene compositions in the 'filling' part of the sandwich experiment, to check that they were indeed the same within analytical error as in the 'bread' layers. Some crystallization in the 'filling' part is inevitable unless the initial glass composition is exactly that expected at equilibrium; in fact, as regards attainment of equilibrium, an absence of crystals in the 'filling' would be an ambiguous result, in the same way that 'no reaction' in the determination of a subsolidus univariant reaction indicates either full equilibrium at the P–T condition or merely sluggish reaction kinetics.

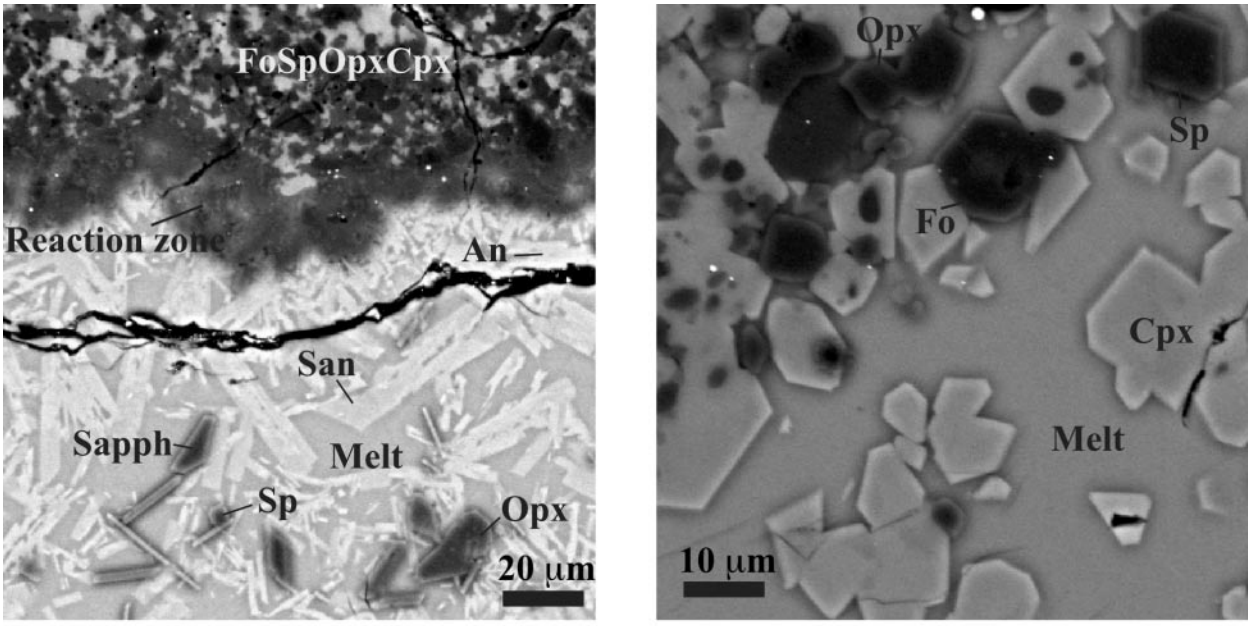

Fig. 2. Electron back-scatter images showing the texture of experiments: (a) C-1576, a disequilibrium sandwich experiment in which the original glass zone, now crystallized to Sp + Opx + An + San + Sapph + Melt, is separated from the Fo + Opx + Cpx + Sp zone by a layer of Opx (labelled 'Reaction zone'); (b) C-1448, a typical experiment in which equilibrium between the original zones is inferred. (See Table 3 for experimental conditions and Table 4 for phase compositions.)

Clearly, a key aspect of any partial melting experiment in which the melt is separated from the crystals is demonstration of equilibrium between melt and crystals. We shall point to some other runs where we believe such equilibrium was not obtained, based on the following criteria (as discussed above): (1) careful examination of the interface between the melt-rich and the crystal-rich parts; (2) comparison of compositions of solid-solution phases in the two parts. On the basis of these criteria, equilibrium was obtained in the majority of the sandwich experiments reported here. Application of these criteria may not be possible in diamond-aggregate or similar types of melt extraction experiments, in which case the results from these experiments must be viewed with a degree of caution.

Several lines of evidence indicate that local equilibrium was approached closely in the experiments of this study. In addition to being the same in different parts of the sandwich, the compositions of Opx and Cpx are generally fairly homogeneous: the most heterogeneous oxide component, Al_2O_3, in the most heterogeneous phase, Cpx, generally has a variation of <0·5 wt % one standard deviation, which is comparable with that observed in other simple-system experiments. The amounts of Al_2O_3 in both Opx and Cpx show small but smooth variations with temperature, and are in good agreement with the results of previous studies (see below). Similarly, the average difference between temperatures calculated from the Ca-geothermometer of Nickel *et al.* (1985) and the nominal experimental temperatures is only 23°C, consistent with equilibrium Ca exchange between Opx and Cpx.

The achievement of local equilibrium in this work is expected because the duration of our experiments is generally longer than that used in previous comparable studies. The results of previous near-liquidus experiments in the system CMAS (Presnall *et al.*, 1978; Sen & Presnall, 1984; Liu & Presnall, 1990) suggested that a period of several hours is all that is required to establish reversals of phase boundaries. Walter & Presnall's (1994) experiments in the system CMAS–Na_2O found that 48 h was long enough for the attainment of equilibrium at solidus temperatures. Most of our run durations were longer than this.

EXPERIMENTAL RESULTS

Table 3 summarizes the starting materials, the run conditions, the techniques used, and the results in terms of phases present, for each experiment. The compositions of these phases are given in Table 4. Calculated temperatures from the two-pyroxene geothermometer of Nickel *et al.* (1985) for those experiments containing both Opx and Cpx are shown in Table 3. There is a good

Table 4: Composition data from electron microprobe analyses (for run conditions, see Table 3)

		CaO	MgO	Al_2O_3	SiO_2	K_2O
DEs						
C-1111, 1330°C	Fo(10)	0·28(0·03)	57·16(0·11)	0·00(0·00)	42·57(0·11)	—
	Sp(7)	0·11(0·06)	28·43(0·10)	71·45(0·11)	0·00(0·00)	—
	Opx(8)	2·16(0·16)	34·78(0·33)	9·25(0·20)	3·82(0·20)	—
	Melt(8)	13·97(0·28)	16·16(0·45)	20·74(0·19)	49·13(0·12)	—
C-1556, 1310°C	Fo(14)	0·28(0·06)	56·78(0·12)	0·17(0·05)	42·67(0·16)	—
	Sp(13)	0·10(0·06)	28·91(0·14)	70·83(0·13)	0·16(0·12)	—
	Opx(22)	2·10(0·14)	35·03(0·19)	8·46(0·39)	54·41(0·27)	—
	Melt(14)	14·34(0·27)	15·73(0·36)	20·14(0·31)	49·79(0·25)	—
C-1555, 1300°C	Fo(12)	0·30(0·05)	56·79(0·18)	0·20(0·06)	42·72(0·14)	—
	Sp(14)	0·10(0·08)	28·99(0·17)	70·70(0·18)	0·22(0·14)	—
	Opx(20)	2·11(0·13)	34·86(0·21)	8·48(0·39)	54·55(0·30)	—
	Cpx(21)	18·63(0·29)	20·73(0·30)	8·81(0·29)	51·84(0·26)	—
	Melt*					
KEs						
C-1417, 1330°C	Fo(14)	0·32(0·03)	56·72(0·13)	0·00(0·00)	42·96(0·12)	—
	Sp(15)	0·12(0·03)	28·46(0·09)	71·42(0·09)	0·00(0·00)	—
	Melt(24)	14·17(0·07)	15·47(0·11)	20·36(0·06)	49·41(0·14)	0·59(0·02)
C-1423, 1320°C	Fo(12)	0·33(0·04)	56·96(0·11)	0·00(0·00)	42·72(0·12)	—
	Sp(17)	0·08(0·04)	28·42(0·11)	71·51(0·11)	0·00(0·00)	—
	Melt(12)	14·64(0·07)	14·91(0·07)	20·40(0·08)	49·43(0·11)	0·63(0·02)
C-1422, 1310°C	Fo(18)	0·31(0·03)	56·78(0·11)	0·00(0·00)	42·91(0·11)	—
	Sp(13)	0·13(0·08)	28·35(0·09)	71·52(0·10)	0·00(0·00)	—
	Opx(19)	2·47(0·41)	34·36(0·32)	8·60(0·34)	54·57(0·27)	—
	Cpx(19)	18·22(0·40)	21·15(0·26)	8·67(0·42)	51·96(0·30)	—
	Melt(19)	14·60(0·07)	14·30(0·07)	20·39(0·10)	49·98(0·11)	0·73(0·03)
C-1461, 1310°C	Fo(8)	0·29(0·03)	56·72(0·04)	0·00(0·00)	42·99(0·06)	—
	Sp(8)	0·08(0·04)	28·56(0·12)	71·28(0·10)	0·08(0·04)	—
	Opx(21)	2·23(0·17)	34·84(0·30)	8·34(0·42)	54·59(0·33)	—
	Cpx(21)	18·44(0·35)	21·00(0·40)	8·39(0·34)	52·17(0·26)	—
	Melt(15)	12·87(0·14)	12·75(0·13)	20·55(0·16)	51·52(0·13)	2·31(0·07)
C-1448, 1300°C	Fo(9)	0·30(0·05)	56·71(0·19)	0·09(0·13)	42·89(0·15)	—
	Sp(8)	0·14(0·06)	28·51(0·07)	71·25(0·16)	0·10(0·09)	—
	Opx(19)	2·19(0·30)	34·80(0·36)	8·50(0·40)	54·51(0·37)	—
	Cpx(19)	18·30(0·47)	20·90(0·42)	8·58(0·43)	52·22(0·35)	—
	Melt(20)	11·19(0·13)	10·09(0·11)	21·47(0·12)	53·17(0·15)	4·08(0·09)
C-1460, 1290°C	Fo(7)	0·30(0·03)	56·71(0·09)	0·03(0·06)	42·96(0·09)	—
	Sp(13)	0·11(0·07)	28·45(0·12)	71·15(0·24)	0·30(0·19)	—
	Opx(20)	2·10(0·26)	34·99(0·32)	8·19(0·39)	54·72(0·24)	—
	Cpx(23)	18·71(0·38)	20·76(0·45)	8·28(0·45)	52·24(0·39)	—
	Melt(14)	10·43(0·11)	9·36(0·23)	21·60(0·21)	53·85(0·17)	4·76(0·15)
C-1447, 1280°C	Fo(6)	0·28(0·05)	57·00(0·18)	0·00(0·00)	42·73(0·21)	—
	Sp(6)	0·08(0·04)	28·47(0·13)	71·32(0·21)	0·13(0·11)	—
	Opx(15)	2·19(0·30)	34·83(0·54)	8·33(0·58)	54·64(0·38)	—
	Cpx(15)	18·28(0·45)	21·17(0·62)	8·27(0·56)	52·29(0·38)	—
	Melt(11)	8·93(0·17)	7·33(0·14)	21·74(0·35)	55·83(0·28)	6·17(0·11)
C-1574, 1270°C	Fo(11)	0·27(0·07)	56·46(0·14)	0·36(0·11)	42·91(0·11)	—
	Sp(12)	0·09(0·04)	29·09(0·13)	70·43(0·30)	0·39(0·25)	—

		CaO	MgO	Al_2O_3	SiO_2	K_2O
	Opx(18)	2·19(0·29)	34·97(0·32)	8·28(0·56)	54·56(0·40)	—
	Cpx(17)	18·86(0·58)	20·70(0·52)	8·31(0·49)	52·13(0·43)	—
	Melt(13)	6·35(0·13)	5·12(0·09)	20·93(0·12)	59·25(0·18)	8·35(0·12)
C-1585, 1260°C	Fo(7)	0·27(0·03)	56·58(0·14)	0·29(0·09)	42·86(0·16)	—
	Sp(9)	0·05(0·03)	29·05(0·11)	70·58(0·10)	0·31(0·07)	—
	Opx(15)	1·74(0·15)	35·16(0·24)	8·12(0·42)	54·98(0·32)	—
	Cpx(17)	18·97(0·56)	20·79(0·48)	8·09(0·46)	52·16(0·34)	—
	Melt(14)	6·81(0·14)	6·20(0·12)	20·80(0·09)	57·69(0·18)	8·49(0·11)
C-1779, 1250°C	Sp(13)	0·04(0·04)	28·70(0·12)	71·04(0·18)	0·21(0·08)	—
	Opx(22)	1·79(0·17)	34·62(0·22)	9·36(0·52)	54·24(0·33)	—
	Cpx(18)	20·03(0·45)	19·16(0·43)	9·67(0·48)	51·14(0·31)	—
	San(15)	2·81(0·43)	0·00(0·00)	20·81(0·38)	62·29(0·42)	14·08(0·40)
	Melt(22)	5·44(0·15)	4·22(0·17)	22·16(0·12)	58·08(0·30)	10·09(0·20)
C-1701, 1240°C	Sp(12)	0·07(0·05)	28·69(0·11)	70·99(0·27)	0·25(0·18)	—
	Opx(19)	1·71(0·10)	34·66(0·19)	9·30(0·45)	54·33(0·29)	—
	Cpx(3)†	18·91(1·08)	20·21(1·83)	9·97(1·71)	50·78(2·22)	0·14(0·16)
	An(6)	15·21(0·34)	0·77(0·18)	31·14(0·38)	49·69(0·31)	3·20(0·28)
	Melt(12)	6·15(0·16)	4·39(0·15)	20·77(0·18)	59·53(0·28)	9·17(0·12)
C-1708, 1230°C	Sp(14)	0·05(0·05)	28·73(0·16)	71·00(0·17)	0·22(0·13)	—
	Opx(22)	1·86(0·17)	34·74(0·19)	8·93(0·45)	54·47(0·33)	—
	Cpx(22)	20·27(0·42)	19·03(0·33)	9·55(0·38)	51·15(0·26)	—
	An(8)	14·09(0·65)	0·63(0·28)	30·46(0·49)	50·80(0·64)	4·02(0·54)
	San(20)	3·10(0·38)	0·00(0·00)	21·14(0·40)	61·95(0·42)	13·81(0·38)
	Melt(10)	5·41(0·11)	3·90(0·09)	21·04(0·11)	59·54(0·23)	10·12(0·11)
C-1580, 1250°C	Solid region					
	Fo(12)	0·24(0·08)	56·48(0·26)	0·28(0·15)	42·99(0·20)	—
	Sp(11)	0·09(0·06)	28·63(0·10)	71·12(0·13)	0·16(0·10)	—
	Opx(16)	2·08(0·29)	34·82(0·39)	8·67(0·58)	54·53(0·42)	—
	Cpx(17)	18·94(0·69)	20·58(0·57)	8·58(0·39)	51·91(0·39)	—
	Glass region					
	An(9)	12·45(0·93)	0·41(0·27)	28·59(0·67)	52·98(0·93)	5·58(0·77)
	San(9)	2·66(0·16)	0·00(0·00)	20·38(0·14)	62·83(0·17)	13·82(0·18)
	Sapph(9)	0·28(0·14)	23·99(0·41)	57·14(0·64)	18·59(0·78)	—
	Melt(14)	4·20(0·10)	3·23(0·11)	20·05(0·07)	63·19(0·21)	9·33(0·17)
C-1576, 1230°C	Solid region					
	Fo(14)	0·24(0·04)	56·49(0·19)	0·22(0·06)	43·06(0·16)	—
	Sp(13)	0·10(0·04)	28·60(0·13)	71·07(0·11)	0·23(0·07)	—
	Opx-1(10)	2·04(0·31)	34·83(0·43)	8·72(0·49)	54·41(0·38)	—
	Cpx(14)	18·69(0·57)	20·54(0·53)	8·65(0·45)	52·12(0·43)	—
	Glass region					
	Sp(9)	0·10(0·05)	28·70(0·11)	70·99(0·14)	0·21(0·05)	—
	Opx-2(6)	0·72(0·04)	33·40(0·48)	14·11(0·54)	51·76(0·13)	—
	An(5)	12·52(1·02)	0·15(0·03)	29·73(0·89)	52·44(1·10)	5·51(0·84)
	San(8)	3·23(0·33)	0·05(0·06)	21·18(0·31)	62·13(0·43)	13·41(0·26)
	Sapph(9)	0·26(0·04)	24·51(0·49)	54·82(0·65)	20·40(0·39)	—
	Melt(12)	3·47(0·11)	2·55(0·11)	18·61(0·12)	66·39(0·26)	8·98(0·10)
REs-1						
C-1621, 1340°C	Melt(8)	15·60(0·12)	15·06(0·09)	19·88(0·12)	49·46(0·16)	—
C-1639, 1320°C	Sp(6)	0·14(0·07)	28·84(0·14)	70·78(0·15)	0·25(0·14)	—
	Opx(13)	2·36(0·26)	34·31(0·38)	9·04(0·43)	54·29(0·22)	—

Table 4: continued

		CaO	MgO	Al_2O_3	SiO_2	K_2O
	Cpx(16)	18·19(0·51)	21·22(0·42)	9·07(0·41)	51·52(0·36)	—
	Melt(8)	15·42(0·16)	14·28(0·14)	20·45(0·09)	49·85(0·10)	—
C-1565, 1320°C	Sp(9)	0·24(0·14)	28·98(0·17)	70·31(0·38)	0·48(0·37)	—
	Opx(16)	2·35(0·21)	34·26(0·27)	9·82(0·62)	53·57(0·48)	—
	Cpx(31)	18·20(0·41)	20·99(0·36)	9·78(0·46)	51·04(0·36)	—
	An(11)	20·24(0·13)	0·74(0·18)	34·65(0·35)	44·37(0·26)	—
	Melt(14)	15·51(0·24)	14·13(0·12)	20·76(0·08)	49·60(0·14)	—
C-1566, 1310°C	Opx(14)	2·33(0·07)	35·06(0·25)	7·47(0·68)	55·14(0·43)	—
	Cpx(15)	18·63(0·33)	21·19(0·39)	7·99(0·64)	52·19(0·36)	—
	An(9)	20·26(0·14)	0·88(0·17)	34·66(0·28)	44·21(0·26)	—
	Melt*					
REs-2						
C-1769, 1340°C	Fo(13)	0·30(0·04)	56·54(0·14)	0·21(0·07)	42·95(0·17)	—
	Melt(16)	14·38(0·12)	16·70(0·09)	19·37(0·07)	49·55(0·12)	—
C-1767, 1320°C	Fo(12)	0·29(0·05)	56·51(0·22)	0·14(0·09)	43·07(0·17)	—
	Opx(21)	2·30(0·17)	34·82(0·33)	7·74(0·77)	55·14(0·42)	—
	Melt(19)	15·14(0·11)	15·41(0·11)	19·90(0·11)	49·54(0·13)	—
C-1781, 1315°C	Fo(13)	0·26(0·05)	56·53(0·13)	0·18(0·08)	43·03(0·10)	—
	Sp(12)	0·10(0·06)	28·63(0·06)	71·08(0·16)	0·19(0·10)	—
	Opx(22)	2·25(0·15)	34·34(0·25)	9·19((0·45)	54·22(0·25)	—
	Cpx(22)	18·47(0·47)	20·87(0·43)	9·14(0·41)	51·52(0·31)	—
	Melt(16)	15·35(0·12)	14·82(0·07)	20·35(0·12)	49·48(0·15)	—
C-1768, 1310°C	Fo(14)	0·26(0·05)	56·49(0·14)	0·14(0·06)	43·10(0·13)	—
	Sp(8)	0·05(0·04)	28·44(0·12)	71·51(0·13)	0·00(0·00)	—
	Opx-1(13)	2·26(0·14)	34·34(0·18)	9·11(0·38)	54·28(0·19)	—
	Cpx-1(14)	17·54(0·89)	21·53(1·08)	9·47(0·83)	51·46(0·49)	—
	Glass region					
	Sp(10)	0·20(0·07)	28·51(0·10)	70·79(0·26)	0·50(0·21)	—
	Opx-2(22)	2·45(0·21)	34·61(0·24)	7·87(0·44)	55·07(0·34)	—
	Cpx-2(15)	18·55(0·36)	21·00(0·34)	8·48(0·25)	51·96(0·23)	—
	An(18)	19·85(0·17)	0·74(0·21)	35·21(0·32)	44·19(0·23)	—
C-1789, 1300°C	Fo(11)	0·30(0·06)	56·54(0·13)	0·16(0·04)	42·99(0·14)	—
	Sp*					
	Opx(17)	2·19(0·46)	34·80(0·45)	8·87(0·40)	54·14(0·41)	—
	Cpx(17)	18·81(0·34)	20·25(0·26)	9·70(0·53)	51·24(0·37)	—

The number in parenthesis after the name of the phase is the number of successful analyses performed on that phase. Data reading: 0·28(0·03) is 0·28 ± 0·03. All analyses were normalized to 100 wt % before averages and standard deviation were calculated.
*Phase is confirmed but too small to analyse.
†Phase is confirmed but only poor quality analyses are available.

correlation between calculated and experimental temperatures, although with a systematic offset towards the calculated temperatures being higher at low experimental temperatures, with a mean difference of 23°C (see Fig. 5).

The initial DEs bracket the solidus in the system CMAS between 1300°C (C-1555) and 1310°C at 1·1 GPa. The run at 1300°C contains a small amount of melt (too small to analyse). The melt may have been produced as a result of H_2 diffusion into the capsule during the run, producing a trace of water by reducing SiO_2 to Si, which alloys with Pt (Chen & Presnall, 1975). At slightly higher temperature (1310°C, C-1556), one

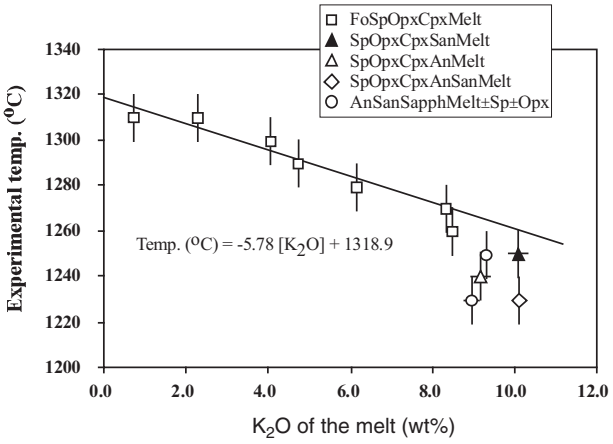

Fig. 3. Relationship between nominal experimental temperature and K_2O content of melt for the KEs. The uncertainty in experimental temperatures is assumed to be ±10°. A linear correlation between nominal experimental temperature and K_2O content of the melt is observed at low K_2O contents (<8·5 wt %) for melts in equilibrium with the Sp-lherzolite phase assemblage. The solidus temperature of 1319°C for the Sp-lherzolite phase assemblage in the system CMAS at 1·1 GPa was obtained by linear regression of K_2O vs T for experiments with K_2O <7 wt %, and extrapolating the resulting regression parameters to zero K_2O.

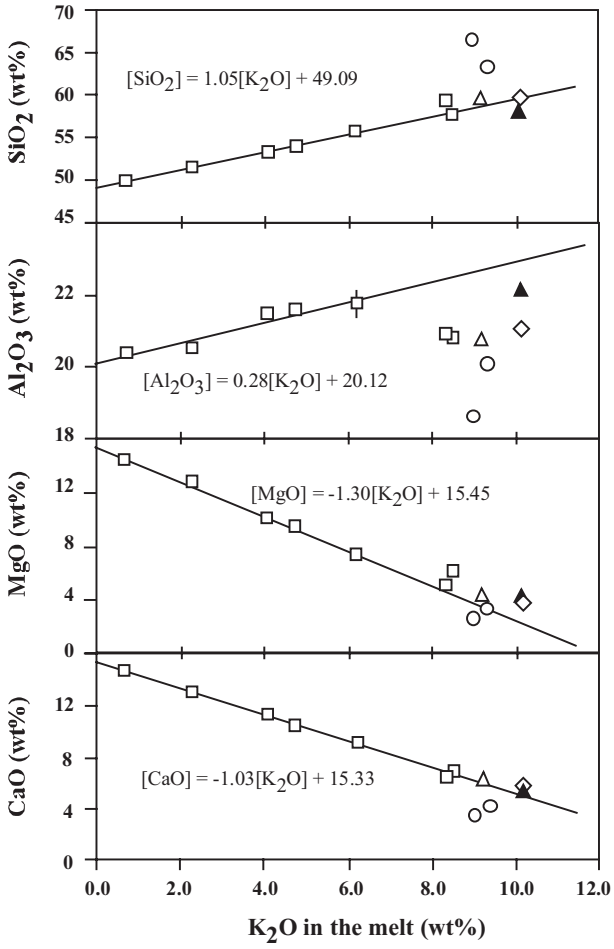

Fig. 4. Variation diagram showing oxide trends for melts in the KEs. Symbols as in Fig. 3. One standard deviation of the oxide content is only occasionally larger than the symbols. There is a strong linear correlation between each of SiO_2, Al_2O_3, MgO, and CaO with K_2O. Linear extrapolation of the data at <7 wt % K_2O to zero K_2O yields the solidus melt composition of 49·09 wt % SiO_2, 20·12 wt % Al_2O_3, 15·45 wt % MgO and 15·33 wt % CaO.

phase (Cpx) disappears in agreement with the phase rule. We did not observe the four solid phases coexisting with melt over a range of temperature (~20°), as did Presnall (1976) and Presnall *et al.* (1979). This is consistent with only small amounts of chemical impurities (such as H_2O) in our run products, and minimal temperature gradients.

Fourteen experiments were carried out using the K_2O-addition method (KEs). The full Sp-lherzolite assemblage coexisting with melt is observed in seven experiments between 1260 and 1310°C. The temperatures of these KEs are plotted against the K_2O contents of the melts in Fig. 3. Within experimental uncertainty the relationship is linear, at least to 8 wt % K_2O and 1270°C. Extrapolating K_2O to zero gives a solidus temperature of 1319°C for the system CMAS. The change of melt composition with K_2O is shown in Fig. 4. On a simple oxide weight percent (wt %) basis, SiO_2 increases linearly with K_2O, MgO and CaO both decrease linearly, and Al_2O_3 remains approximately constant, although in detail it appears to go up then down, with a maximum at ~6 wt % K_2O. The melt composition at the solidus in the CMAS system is found by extrapolation to zero K_2O, as for the solidus temperature: we obtain (in wt %) SiO_2 49·09, Al_2O_3 20·14, MgO 15·45 and CaO 15·33. The compositions of both Opx and Cpx at the CMAS solidus can be deduced similarly (see Table 5).

We then tested these results by making up a glass with this composition and locating its liquidus and solidus (REs-1). The experiment at 1340°C was above the liquidus, whereas two runs at 1320°C (C-1639 and C-1565) crystallized Sp + Opx + Cpx ± An, with the residual melt being close to that in the starting material (Table 4). The compositions of the pyroxenes in C-1639 are in good agreement with the forward experiments, whereas those in C-1565, with a shorter run time and An present, have slightly higher Al_2O_3 (Table 4). These experiments confirm directly the peritectic nature of the melting reaction, as Fo was not crystallized. They also imply that the solidus of the phase assemblage Sp + Opx + Cpx + An is only slightly lower than that of the phase assemblage Fo + Sp + Opx + Cpx, in agreement with Kushiro (1972). Thus the run at 1310°C (C-1566) is almost completely crystallized. Although in one experiment (C-1565) melt coexists with four crystalline phases, the temperature interval over which this occurs is clearly very

Table 5: Compositions of Melt, Opx and Cpx in the system CMAS at 1·0 GPa or 1·1 GPa in the isobaric invariant assemblages Fo + Sp + Opx + Cpx + Melt and Sp + Opx + Cpx + An + Melt: comparison with literature data

		Fo + Sp + Opx + Cpx + Melt						Sp + Opx + Cpx + An + Melt	
Run no.:		($K_2O = 0$)[1]	C-1781[1]	116-3[2]	116-3[3]	116-3[4]	1-K72[5]	C-1565[1]	2-K72[5]
T (°C):		1319	1315	1350	1350	1350	1350	1320	1345
P (GPa):		1·1	1·1	1·1	1·1	1·1	1·0	1·1	1·0
Melt	SiO_2	49·09	49·48(0·15)		49·13(0·37)	49·30(0·1)	50·10	49·60(0·14)	0·91
	Al_2O_3	20·12	20·35(0·12)		19·72(0·33)	19·20(0·1)	20·93	20·76(0·08)	1·37
	MgO	15·45	14·82(0·07)		15·69(0·41)	16·80(0·1)	16·00	14·13(0·12)	14·82
	CaO	15·33	15·35(0·12)		15·47(0·12)	14·90(0·1)	12·98	15·51(0·24)	12·90
Opx	SiO_2	54·54	54·22(0·25)	54·00(0·3)		53·90(0·65)		53·57(0·48)	
	Al_2O_3	8·57	9·19(0·45)	8·51(0·2)		9·49(0·65)		9·82(0·62)	
	MgO	34·47	34·34(0·25)	35·16(0·2)		34·60(0·25)		34·26(0·27)	
	CaO	2·43	2·25(0·15)	2·33(0·1)		2·17(0·1)		2·35(0·21)	
Cpx	SiO_2	51·97	51·52(0·31)	51·40(0·4)		51·04(0·36)			
	Al_2O_3	8·66	9·14(0·41)	9·50(0·65)		9·78(0·46)			
	MgO	21·06	20·87(0·43)	20·20(0·5)		20·99(0·36)			
	CaO	18·30	18·47(0·47)	19·30(0·25)		18·20(0·41)			

[1]This study; [2]Presnall (1976); [3]Presnall *et al*. (1979); [4]Walter & Presnall (1994); [5]Kushiro (1972). Data from the literature have been renormalized to 100%.

narrow (an infinitely narrow temperature interval is expected from the phase rule).

The REs-1 demonstrate empirically that simple crystallization experiments cannot in practice reverse the partial melting equilibrium when this is peritectic, as here (i.e. the melt is in reaction relationship with Fo). Accordingly, we tried reversal crystallization experiments with added Fo. These experiments (called REs-2) directly constrain the solidus of the Sp-lherzolite phase assemblage in the system CMAS at 1·1 GPa to be ~1315 ± 10°C. The experiment at this temperature, C-1781, produced four crystalline phases plus melt; however, the melt composition is slightly less magnesian than the composition deduced from the KEs (Table 5), and is intermediate between this composition and that in equilibrium with Opx + Cpx + Sp + An. The Al_2O_3 content of the pyroxenes is also slightly higher than in other comparable runs. This raises the question of whether equilibrium between Fo and the 'filling' part of the sandwich was truly established. Clearly, equilibrium was not established in a similar experiment at the slightly lower temperature of 1310°C, C-1768; here the 'filling' crystallized completely to Sp + Opx + Cpx + An, with An separated from Fo by a narrow reaction zone of Opx + Cpx + Sp. The further implications of this experiment for the interpretation of results from melt-extraction experiments (such as the diamond-aggregate technique) will be discussed below.

Table 5 compares the result of this study with previous work in CMAS at similar pressures in the literature. There is a difference of 30°C between the solidus as determined here and the solidus defined by run 116-3 of Presnall (1976), which contains Fo + Opx + Cpx + Sp + Melt at 1350°C and 1·1 GPa. However, another run with the same starting composition reported by Presnall *et al.* (1979), their 122-8 at 1327°C and 1·1 GPa, contained Fo + Opx + Melt and is therefore above the solidus, which would be in agreement with our result. There is also good agreement as regards the solidus melt composition and the solidus pyroxene compositions. It may be noted that Presnall (1976) reported 8·4 ± 0·2 wt % Al_2O_3 for his Opx based on five analyses, but noted two outliers at 9·6 and 5·5 wt % Al_2O_3, indicating that his Opx was somewhat heterogeneous in composition. The higher amount (9·49 wt %) later reported by Walter & Presnall (1994) following re-analysis of this experiment may be due to the inclusion of high-Al_2O_3 outliers. The solidus temperature and melt composition reported by Kushiro (1972) at 1·0 GPa agree slightly less well, the main difference in melt composition being in CaO (Table 5). Kushiro (1972) also reported data for the phase assemblage Sp + Opx + Cpx + An + Melt; in

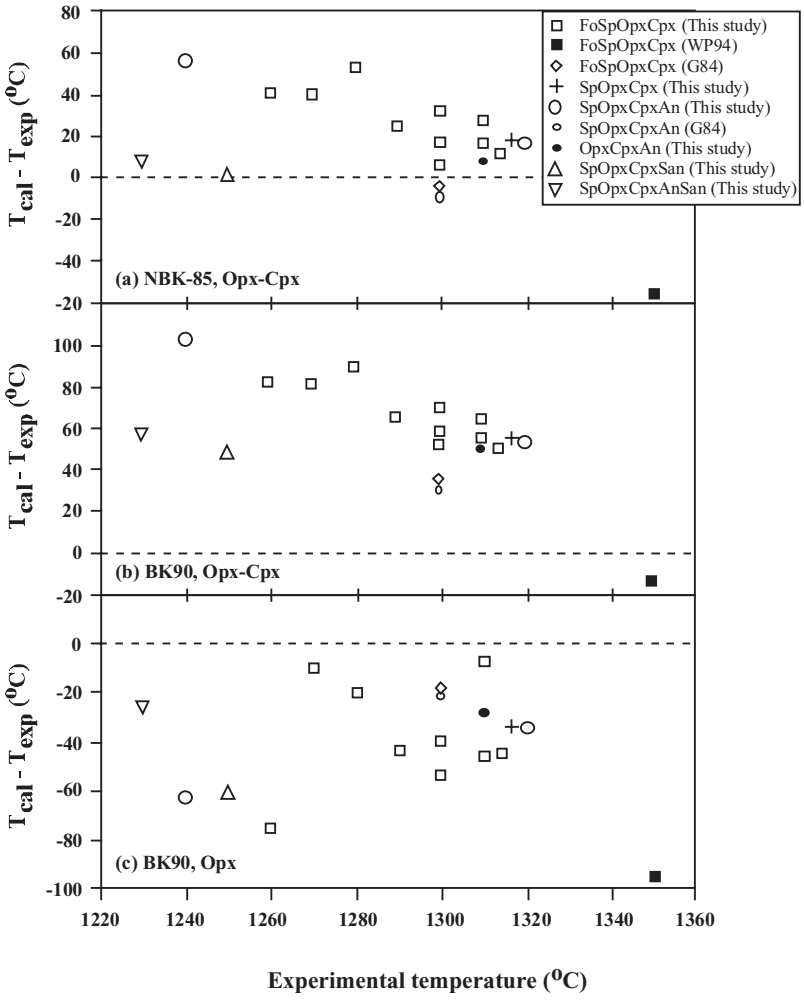

Fig. 5. Temperature difference between the temperatures calculated from two-pyroxene geothermometers and the nominal experimental temperature: (a) the Opx–Cpx geothermometer of Nickel *et al.* (1985); (b) the Opx–Cpx geothermometer of Brey & Kohler [1990; their equation (9)]; (c) the Opx-only geothermometer of Brey & Kohler [1990; their equation (10)]. To show the data clearly, some data points are slightly shifted horizontally. WP94, Walter & Presnall (1994); G84, Gasparik (1984).

agreement with this study, this isobaric invariant point occurs at essentially the same temperature at a melt composition only ~1 wt % lower in MgO than Fo + Sp + Opx + Cpx + Melt.

We attempted to locate the isobaric invariant point in the system CMAS–K_2O by exploring lower temperatures. An isobaric invariant point should exist at which sanidine joins Fo + Opx + Cpx + Sp in equilibrium with melt. Our first attempts consisted of two runs, C-1580 (1250°C) and C-1576 (1230°C), with the same initial melt composition SEM02-08 as used at 1260 and 1270°C. However, this melt composition crystallized An + Sapph + San at 1260°C, joined at 1250°C by Sp and Opx, the latter with very high Al_2O_3 (14 wt %). This assemblage is clearly out of equilibrium with the Fo + Opx + Cpx + Sp layers, with a narrow reaction zone of about 10–20 μm separating the two assemblages (see Fig. 2a).

With this experience, we tried again with a new initial melt composition (SEM02-10). This time equilibrium was approached throughout the charge, but Fo was reacted out, producing Sp + Opx + Cpx + An + Melt (with a trace of residual Fo) in C-1701 at 1240°C, and the isobarically invariant assemblage Sp + Opx + Cpx + An + San + Melt in C-1708 at 1230°C. A third attempt with another initial melt composition (SEM02-13) produced Sp + Opx + Cpx + San + Melt with a trace of residual Fo in C-1779 at 1250°C.

These and the higher-temperature results in the system CMAS–K_2O are summarized in Fig. 6, a projection from Fo + Di onto the An–Or–Qz plane. Although we failed to locate the isobaric invariant point

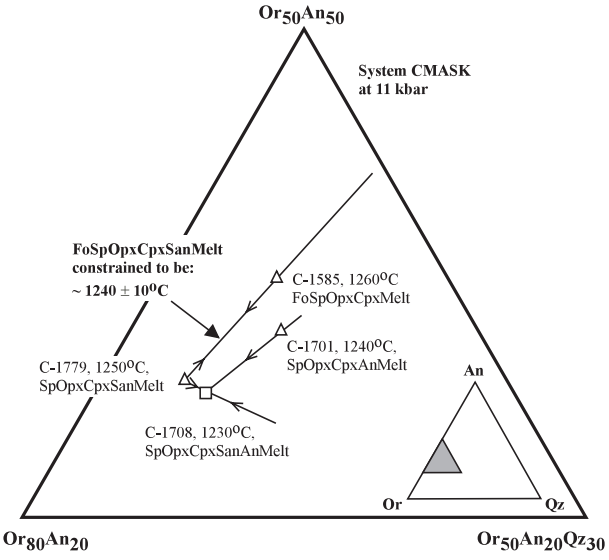

Fig. 6. Defining brackets for the isobaric invariant point Fo + Sp + Opx + Cpx + San + Melt in the system CMAS–K_2O at 1·1 GPa. The melt composition of this invariant point must be located between C-1779 (on the univariant line Sp + Opx + Cpx + San + Melt) and C-1585 (on the univariant line Fo + Sp + Opx + Cpx + An + Melt). Arrows show the direction of fall in temperature. The solidus of this invariant point should be lower than 1250°C but slightly higher than 1230°C, the invariant point Sp + Opx + Cpx + San + An + Melt.

Fo + Sp + Opx + Cpx + San + Melt at 1·1 GPa directly, this point, which is eutectic-like on this projection, must occur at a melt composition between runs C-1585 at 1260°C and C-1779 at 1250°C, at a slightly lower temperature (i.e. ∼1240 ± 10°C).

DISCUSSION

Compositions of Opx and Cpx

The compositions of both Opx and Cpx in the experimental run products vary in CaO and Al_2O_3 contents.

CaO in pyroxenes

The partitioning of CaO between Opx and Cpx is the basis of two-pyroxene geothermometry, the main means of estimating temperatures of equilibration in lherzolitic assemblages. To compare our data with previous work in the system CMAS, we have used the formulation of Nickel *et al.* (1985) to calculate temperatures from our experimental run products (Table 3 and Fig. 5a). The calculated temperatures are in good agreement with nominal experimental temperatures, although in detail there is a weak systematic tendency for the former to be higher at low experimental temperatures. The average difference between the calculated temperature and the nominal experimental temperature for the experiments reported here is 23° with a standard deviation of 17°. We also tested two other pyroxene geothermometers, equations (9) and (10) of Brey & Köhler (1990). Equation (9), which uses the exchange of Ca between Opx and Cpx, yields higher calculated temperatures, with an average difference of 65°C between the calculated temperatures and the experimental temperatures (Fig. 5b). Conversely, equation (10), which uses only the amount of Ca in Opx coexisting with Cpx, gives lower calculated temperatures, with an average difference of −39° (Fig. 5c). These equations were intended for use with chemically complex natural systems, but were formulated as simply as possible for ease of use. Figure 5b and c indicates that this simplicity may result in a loss of accuracy; consequently, more rigorous albeit tediously complicated two-pyroxene geothermometers could potentially give better results.

Shown in Fig. 7 are differences between observed and calculated temperatures using the geothermometer of Nickel *et al.* (1985) for experiments in the system CMAS at pressures from 1 atm to 3·4 GPa, from Longhi (1987), Walter & Presnall (1994), Gudfinnsson & Presnall (1996), Klemme & O'Neill (2000*a*), and this study (CMAS ± K_2O). Similar diagrams using the two geothermometers of Brey & Köhler (1990), their equations (9) and (10), are shown in Fig. 8, with the addition of the CMAS–Na_2O data from Walter & Presnall (1994). These plots raise a number of issues regarding potential problems with the experimental database in the CMAS system, in addition to the problem with the geothermometers. One consideration is the choice of thermocouple. The Nickel *et al.* (1985) and Brey & Köhler (1990) geothermometers are based on experiments by those workers using type B Pt/Rh thermocouples, as in this study, whereas the data from Presnall and co-workers were obtained using W/Re thermocouples. Thus the discrepancy with increasing pressure seen in Figs 7 and 8 may be due to an error in the pressure dependence of the Brey–Köhler geothermometers, or to differences in the effect of pressure on the e.m.f. of Pt/Rh thermocouples compared with W/Re thermocouples.

A further complicating issue is the possibility of oxidation of W/Re thermocouples at lower pressures. To guard against this, Walter & Presnall (1994) used a nitrogen flow at low pressures (≤1·1 GPa) for their experiments in the system CMAS–Na_2O, but this precaution does not appear to have been used in the earlier experiments of Presnall and co-workers in the system CMAS [re-analysed by Walter & Presnall (1994)]. Oxidation of W/Re thermocouples is thought not to be a problem at higher pressures, as collapse of the alumina tubing around the thermocouple wires should prevent entry of air. The calculated temperatures from the lower-pressure experiments with W/Re thermocouples with the N_2 flow agree fairly well with the experiments using Pt/Rh thermocouples. However, earlier low-pressure experiments using W/Re thermocouples but without a N_2 flow

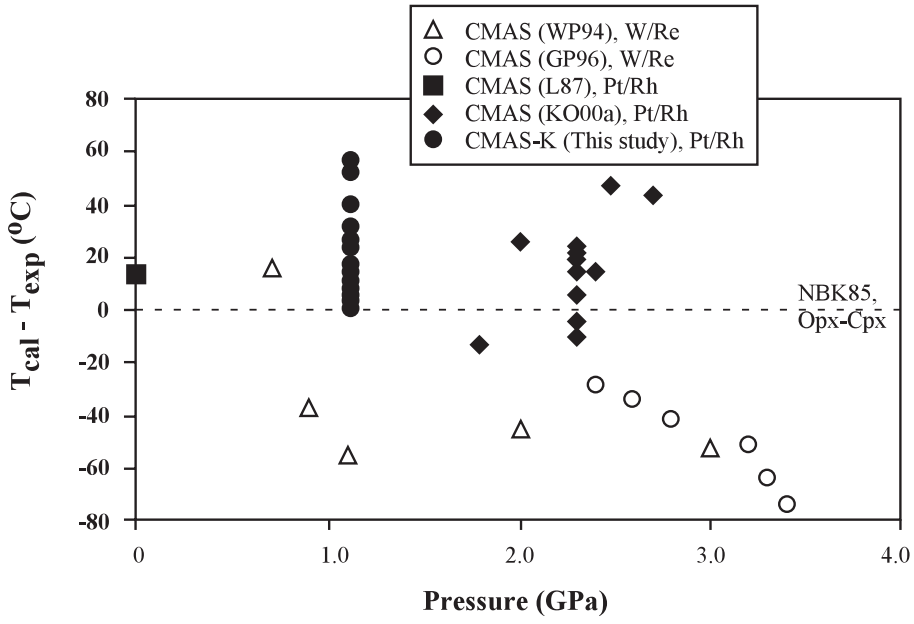

Fig. 7. Difference between experimental temperatures measured using either Pt/Rh or W/Re thermocouples, and calculated temperatures from the Opx–Cpx geothermometer of Nickel *et al.* (1985) for experiments in the systems CMAS and CMAS–K_2O. The data are plotted as a function of the experimental pressure. There is a systematic difference between experimental temperatures measured using Pt/Rh thermocouples (this study; KO00a, Klemme & O'Neill, 2000*a*; L87, Longhi, 1987) and those using W/Re thermocouples (WP94, Walter & Presnall, 1994; GP96, Gudfinnsson & Presnall, 1996). The latter return lower calculated temperatures. It should be noted that the datum at 1 bar using a Pt/Rh thermocouple (from Longhi, 1987), where thermocouple contamination is not likely to be an issue, is consistent with the higher-pressure data using Pt/Rh thermocouples.

(system CMAS) have lower calculated temperatures, consistent with thermocouple drift caused by oxidation.

Al_2O_3 of pyroxenes in Sp-lherzolite

The alumina contents of Opx and Cpx in the Sp-lherzolite assemblage are controlled by the reactions

$$\underset{\text{Opx}}{Mg_2Si_2O_6} + \underset{\text{Sp}}{MgAl_2O_4} = \underset{\text{Opx}}{MgAl_2SiO_6} + \underset{\text{Fo}}{Mg_2SiO_4} \quad (5)$$

and

$$\underset{\text{Cpx}}{CaMgSi_2O_6} + \underset{\text{Sp}}{MgAl_2O_4} = \underset{\text{Cpx}}{CaAl_2SiO_6} + \underset{\text{Fo}}{Mg_2SiO_4}. \quad (6)$$

Previous work has shown that these equilibria are insensitive to pressure but strongly dependent on temperature, Al_2O_3 increasing with rise in temperature (Obata, 1976; Fujii, 1977; Danckwerth & Newton, 1978; Herzberg, 1978; Lane & Ganguly, 1980; Gasparik, 1984; Sen, 1985). Recently Klemme & O'Neill (2000*a*) re-fitted existing experimental data for reaction (5) together with their new data. The alumina contents of Opx coexisting with Fo + Sp in the systems CMAS and CMAS–K_2O reported here agree well with this previous work (Fig. 9b), except for the data of Gudfinnsson & Presnall (1996), which plot at slightly lower values.

The Al_2O_3 contents of Cpx show a very similar trend (Fig. 9a), but with a little more scatter. This extra scatter may be due to a slight pressure effect on this equilibrium, as seen in the experiments of Gasparik (1984). The partitioning of Al between Opx and Cpx does not vary with temperature (i.e. the temperature dependence of the Al isopleths is similar in Opx and Cpx), as demonstrated in Fig. 10. In experiments in the system CMAS–Na_2O, the Cpx might be expected to have additional Al from a jadeite component ($NaAlSi_2O_6$). To test this, we also plotted (Fig. 10b) the data for the CMAS–Na_2O system (Walter & Presnall, 1994) with the molar amount of Al associated with Na subtracted. Remarkably, this results in a greatly increased scatter in the plot, indicating that our expectation of increased Al associated with Na must be incorrect.

Al_2O_3 in pyroxenes, particularly in Cpx, is always the most heterogeneous component in our experiments and anomalous Al_2O_3 contents are a sign of disequilibrium. An example is the subsolidus reversal experiment C-1789, in which the Al_2O_3 of the Cpx remains similar to that in the starting material, although the Opx in this run has changed its Al_2O_3 content to a lower value.

Al_2O_3 in pyroxenes of other phase assemblages

Reactions (5) and (6) show that, in the absence of Fo, the $MgAl_2SiO_6$ (MgTs) component in Opx and the

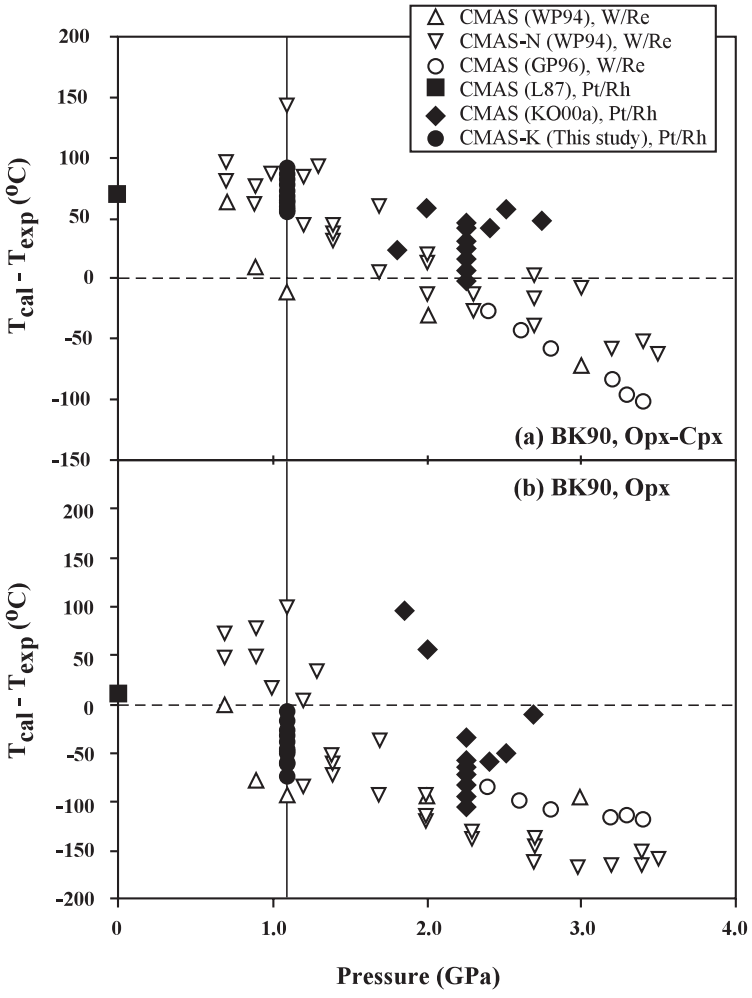

Fig. 8. Comparison of temperature measurement using Pt/Rh thermocouples and W/Re thermocouples in experiments in the systems CMAS, CMAS–K_2O and CMAS–Na_2O, with calculated temperatures from (a) the Opx–Cpx geothermometer of Brey & Kohler (1990) and (b) the Opx-only geothermometer of Brey & Kohler (1990). WP94, Walter & Presnall (1994); GP96, Gudfinnsson & Presnall (1996); L87, Longhi (1987); KO00a, Klemme & O'Neill (2000*a*). A flow of N_2 was used to protect the W/Re thermocouples against oxidation in the low-pressure experiments (<1·1 GPa) in the system CMAS–Na_2O, so that these experiments give similar nominal experimental temperatures to those using Pt/Rh thermocouples.

$CaAl_2SiO_6$ (CaTs) component in Cpx increase. Therefore, the pyroxenes in the phase assemblage Sp + Opx + Cpx should have higher Al_2O_3 contents than those in the phase assemblage Fo + Opx + Cpx + Sp, as observed in our experiments (Fig. 11).

A single governing reaction for the Al_2O_3 content in both pyroxenes coexisting with An + Sp can be written:

$$\underset{\text{Sp}}{MgAl_2O_4} + \underset{\text{An}}{CaAl_2Si_2O_8} = \underset{\text{Opx}}{MgAl_2SiO_6} + \underset{\text{Cpx}}{CaAl_2SiO_6}. \quad (7)$$

The absence of either Sp or An would shift this reaction to the left-hand side so that MgTs in Opx and CaTs in Cpx decrease. Again, this is observed in our experiments (Fig. 11).

As the Al_2O_3 contents of pyroxenes depend on the identities of coexisting phases, the Al_2O_3 contents are useful indicators of equilibrium between the different parts of sandwich experiments. Although this kind of disequilibrium is clearly seen in a few experiments, in most runs the same Al_2O_3 contents in pyroxenes were indeed observed in the 'filling' and the ends of the sandwich.

The effect of K_2O on melting relations of Sp-lherzolite in the system CMAS–K_2O

Effect of K_2O on melt compositions

We find that 1 wt % K_2O in the melt depresses the solidus temperature of the Sp-lherzolite phase assemblage at

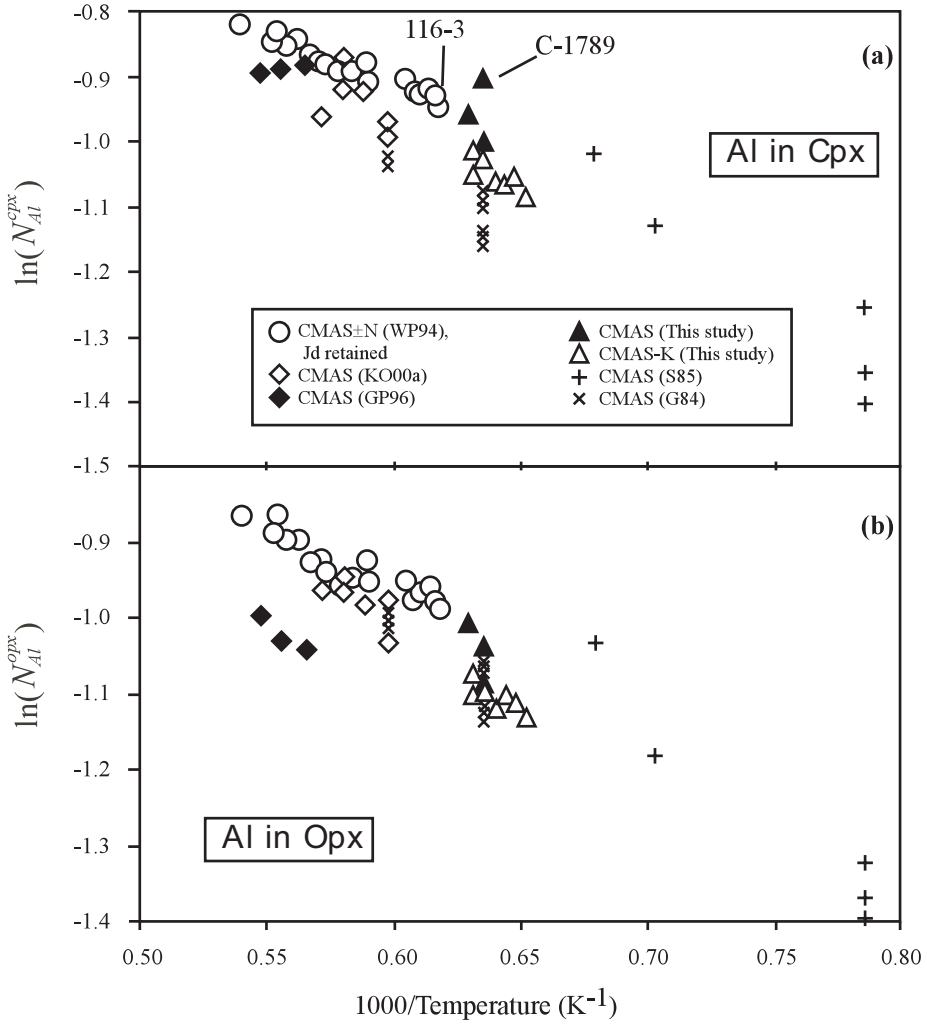

Fig. 9. The solubility of Al in Cpx (a) and Opx (b) plotted as the number of Al cations per formula unit of six oxygens (N_{Al}^{cpx} and N_{Al}^{opx}) vs inverse temperature for the Sp-lherzolite phase assemblage in the systems CMAS, CMAS–K_2O and CMAS–Na_2O. Data sources: WP94, Walter & Presnall (1994); KO00a, Klemme & O'Neill (2000*a*); GP96, Gudfinnsson & Presnall (1996); S85, Sen (1985); G84, Gasparik (1984).

1·1 GPa by about 5·8°C (Fig. 2); concurrently, this amount of K_2O decreases MgO by 1·30% and CaO by 1·03%, but increases SiO_2 by 1·05% and Al_2O_3 by 0·28% (Fig. 3).

To compare the effect of K_2O on melt composition with that of Na_2O, we plot our experimental data in mole percent in Fig. 12, together with the data of Walter & Presnall (1994) in the system CMAS–Na_2O, at 2·0 GPa. Walter & Presnall (1994) provided a global regression of their data to 3·5 GPa that shows that the difference in pressure between 1·1 and 2·0 GPa has a negligible effect in this context. For K, an increase of 1% molar increases Si by 0·95% and Al by 0·33%, and decreases Mg by 1·46% and Ca by 0·82%. For all cations, the effect of Na is similar in direction to that of K, but much weaker: a 1% molar increase in Na only increases Si by 0·1% and Al by 0·1%, and decreases Mg by 0·74% and Ca by 0·47%.

Hence, the effect of K_2O on modifying the composition of melts multiply saturated with Fo + Opx + Cpx + Sp in the system CMAS–K_2O is very different from that of Na_2O in the system CMAS–Na_2O. This is illustrated in Fig. 13, in which the compositions of multiply saturated melts are plotted in the basalt tetrahedron projected from Ol (Fig. 13a) and Di (Fig. 13b). The data for the system CMAS–Na_2O were taken from Walter & Presnall (1994) at 2·0 GPa, the higher pressure being used because Na_2O stabilizes plagioclase at the expense of spinel at only ~2 wt % Na_2O at 1·1 GPa. The difference in the behaviours of K_2O and Na_2O can be summarized under three points, as follows. (1) The addition of K_2O drives the melt composition towards the Qz-normative field (defined by the join AbAnOr–Hy in Fig. 13b), the melt becoming Qz-normative at ~2 wt % K_2O. The addition of Na_2O drives the melt composition towards the Ne-normative

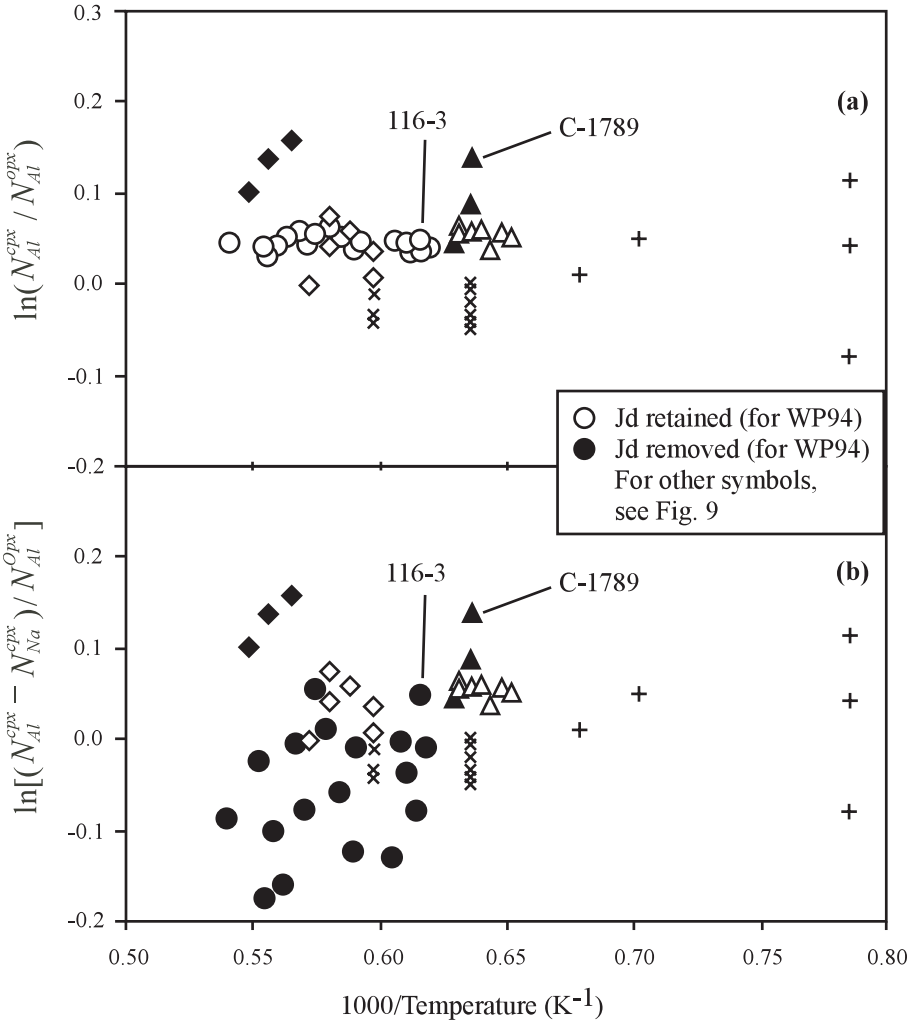

Fig. 10. Partitioning of Al between Cpx and Opx for a Sp-lherzolite phase assemblage in the systems CMAS, CMAS–K_2O and CMAS–Na_2O. The CMAS–IV data are plotted in two ways: (a) with the Al associated with Na as the Jadeite component in Cpx ($NaAlSi_2O_6$: Jd) retained; (b) with this component subtracted. Clearly the latter procedure increases the scatter. (For data sources, see Fig 9.)

field (defined by the join AbAnOr–Ol in Fig. 13b), the melt becoming Ne-normative at ~2 wt % Na_2O. (2) K_2O decreases normative Di, whereas Na_2O has no effect on this normative component. (3) As a consequence, adding K_2O eventually produces a corundum-normative melt at ~8 wt % K_2O. Na_2O-rich melts never become corundum-normative.

Effect of K_2O on the partitioning of MgO between olivine and melt

The amount of MgO in a basaltic magma increases strongly with rise in temperature. Several workers have attempted to quantify this effect, using the partition coefficient for MgO between Melt and Ol (Leeman, 1978; Ford *et al.*, 1983; Gudfinnsson & Presnall, 2001). However, such single-element partition coefficients are generally expected to depend on other factors including the details of the melt composition (e.g. O'Neill & Eggins, 2002). Figure 14 shows that adding K_2O to CMAS produces a very different trend from that established by the systems CMAS, CMAS–Na_2O and CMAS–FeO (compare Gudfinnsson & Presnall, 2001, fig. 2). Clearly, empirical geothermometers, with a less than rigorous thermodynamic basis, have limited reliability, and should never be applied to compositions outside those used in their formulation.

The MgO-partitioning 'magmathermometer' of Ford *et al.* (1983) has been used recently by Danyushevsky *et al.* (1996), Falloon *et al.* (1999, 2001) and Falloon & Danyushevsky (2000). Falloon & Danyushevsky (2000) found that this formulation returns progressively larger errors in the calculated liquidus temperatures of basaltic melts as alkalis ($Na_2O + K_2O$) exceed 3 wt %. Our data

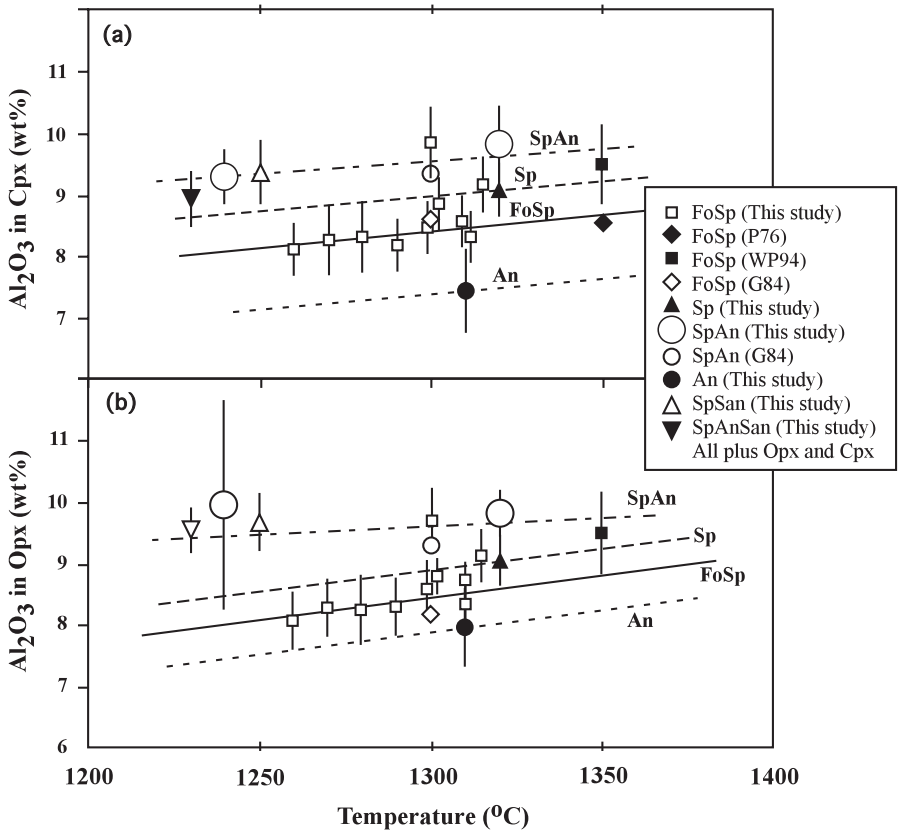

Fig. 11. The effect of the coexisting phase assemblage on the solubility of Al_2O_3 in Cpx (a) and in Opx (b) from phase assemblage to phase assemblage. Lines are fitted by eye. Some data are slightly shifted horizontally to display them more clearly.

can be used to check this phenomenon further. The result is shown in Fig. 15. Apparently the Ford *et al.* (1983) geothermometer cannot reproduce the experimental temperatures accurately either in the system CMAS or in the system CMAS–K_2O (Fig. 15a). We also checked the effect of pressure on the geothermometer, with results shown in Fig. 15b. Evidently pressure affects the calculated temperature as well.

Melt properties and phase relations

The CIPW norms of the experimentally observed melt compositions are summarized in Table 6. Melts with K_2O contents below ~4·1 wt % K_2O are *ol*-normative. The melt becomes *qz*-normative at higher K_2O. Melts with >8 wt % K_2O are *co*-normative.

Melt compositions observed in this study are plotted in Fig. 16. In the system CMAS there are two isobaric invariant points of interest, A (Fo + Sp + Opx + Cpx + Melt) and A* (Sp + Opx + Cpx + An + Melt). Points B, C and D are isobaric invariant points in the system CMAS–K_2O, for the phase assemblages Fo + Sp + Opx + Cpx + San + Melt, Sp + Opx + Cpx + An + San + Melt and Sp + Opx + An + San + Sapph + Melt, respectively. All these invariant points are peritectic. From point A to point B the isobarically univariant phase assemblage is Fo + Sp + Opx + Cpx + Melt, whereas from point B to point C it is Sp + Opx + Cpx + San + Melt. At point C, the melt composition trend is joined by another melt composition trend emanating from point A*, with the isobarically univariant phase assemblage of Sp + Opx + Cpx + An + Melt. The isobarically univariant phase assemblage from point C to point D is Sp + Opx + San + An + Melt. Thermal maxima must be located between B and C, and between C and D. The temperature change is judged by our direct temperature observation or by the method of Presnall (1986). One interesting property of the system suggested by our experiments is that the univariant solidus curves have a relatively steep temperature drop (1320–1240°C) from A to B or from A* to C, but the temperature interval between A and A* and the corresponding univariant solidus curves A–B and A*–C is very small.

The compositions of Melt, Cpx and Opx in the experiments with the phase assemblage Fo + Sp + Opx + Cpx + Melt in the system CMAS–K_2O were fitted by regression to a second-degree polynomial of the form

$$X_i^{\phi} = AT^2 + BT + C$$

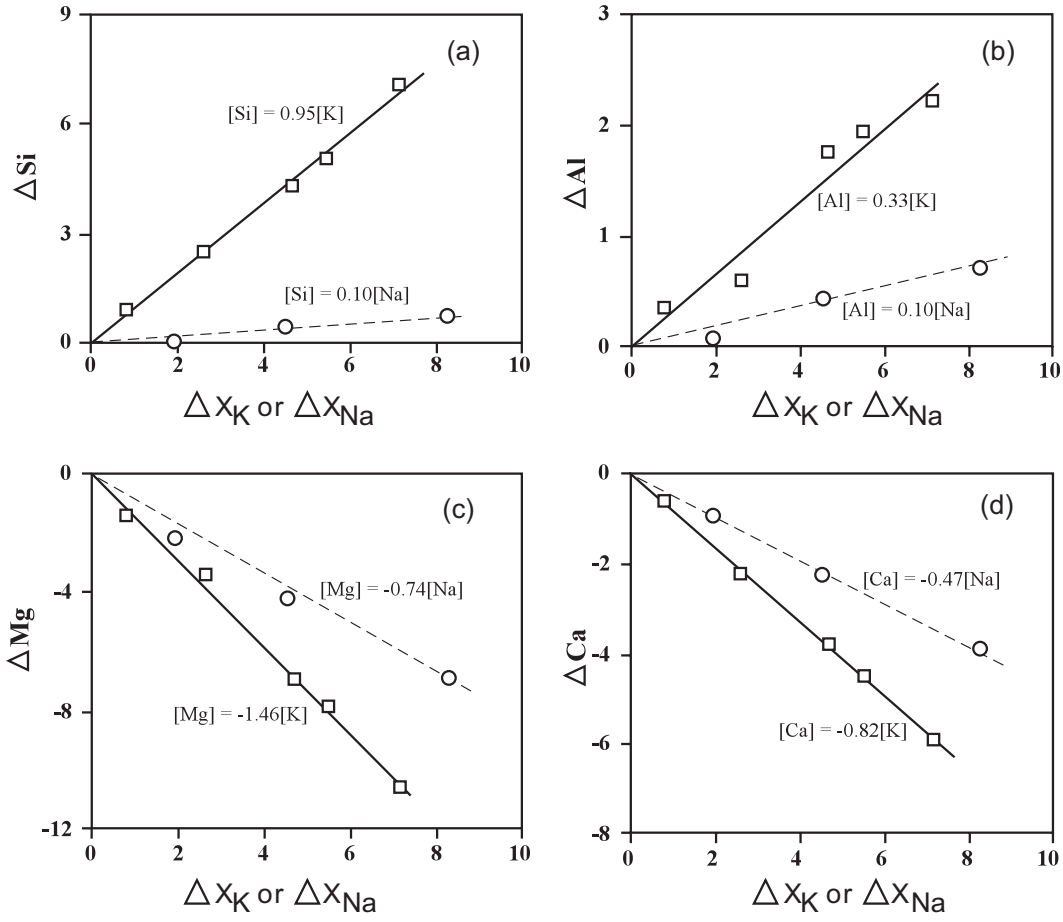

Fig. 12. The change in the molar amounts of each cation (Si, Al, Mg and Ca) in the melt relative to pure CMAS with the addition of either K or Na. Data are plotted in mole percent. The data for CMAS–K_2O are from this study and for CMAS–Na_2O from Walter & Presnall (1994). Bold continuous line indicates system CMAS–K_2O at 1·1 GPa (this study); fine dashed line indicates system CMAS–Na_2O at 2·0 GPa from Walter & Presnall, (1994). The addition of both K and Na increases the Si and Al contents of the melt, and decreases the Mg and Ca contents, but the effect of K is much stronger than that of Na, especially when considered on a molar rather than weight percent basis.

where X_i^ϕ is the concentration in weight percent of oxide i in phase ϕ and T is in °C.

To calculate the partial melting reaction along the univariant curve Fo + Sp + Opx + Cpx + Melt, the method of Walter *et al.* (1995) is used. The melting reaction is independent of the bulk composition as long as all phases are present. The calculated reaction coefficients are plotted against temperature in Fig. 17. The partial melting reactions for some special temperatures are listed in Table 8.

Also listed in Table 8 are the partial melting reactions at the invariant points of the system CMAS (points A and A* in Fig. 16) and the invariant points of the system CMAS–K_2O (points B, C and D in Fig. 16) which are directly calculated from the experimentally observed phase compositions using the method of Korzhinskii (1959).

Partial melting is always peritectic along the univariant curve Fo + Sp + Opx + Cpx + Melt at 1·1 GPa in the system CMAS–K_2O (Fig. 17). At high temperatures (from 1320°C down to 1265°C), Fo is in reaction relationship with melt. From 1276°C Sp becomes in reaction relationship.

Experiment C-1768: an analogue of a diamond-aggregate melt extraction experiment

Run C-1768 is a crystallization experiment on the melt composition determined for the isobaric invariant point Fo + Sp + Opx + Cpx + Melt from the KEs, with additional Fo added in the sandwich geometry. Importantly, this particular run is at 1310°C, just below the solidus (1320°C). The experimental charge was prepared with layers of Fo sandwiching a layer of crushed glass of the anticipated solidus melt composition (synthesized at 1 atm). Initially, of course, both layers have considerable

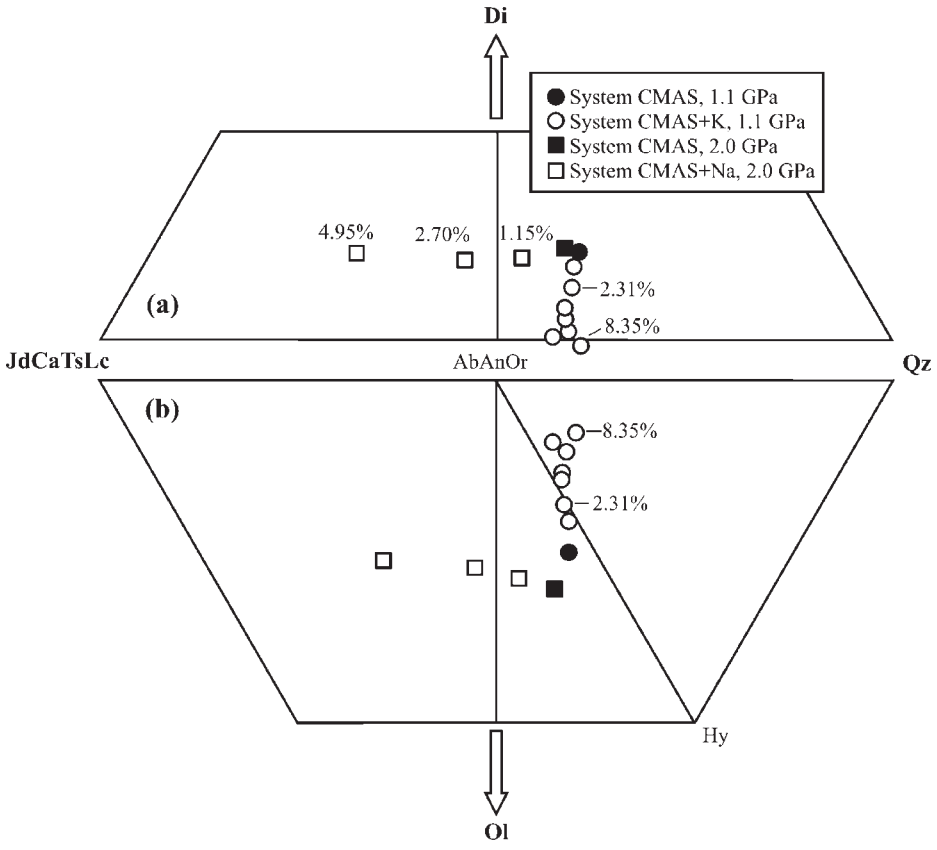

Fig. 13. A comparison of the effects of K_2O and Na_2O in modifying melt compositions: (a) projection of Di–JdCaTsLc–Qz from Ol (molar); (b) projection of Ol–JdCaTsLc–Qz from Di (molar). The plotting procedure is from Falloon & Green (1988). Data in the system CMAS at 1·1 GPa and 2·0 GPa and in CMAS–Na_2O at 2·0 GPa are from Walter & Presnall (1994). Data in the system CMAS–K_2O at 1·1 GPa are from this study.

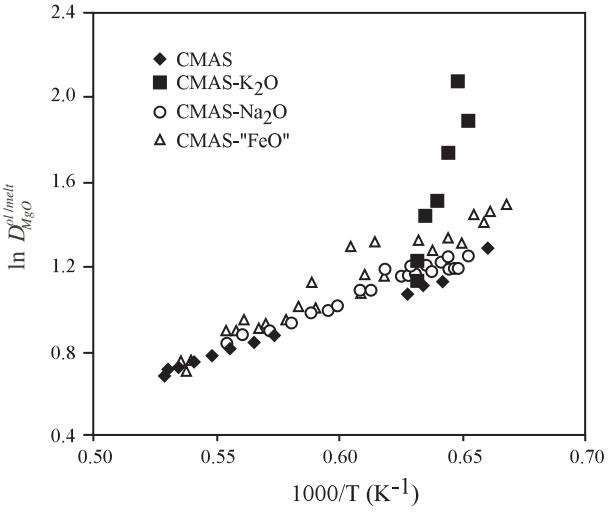

Fig. 14. The effect of K_2O on the molar partitioning of MgO between forsterite and melt as a function of reciprocal temperature. Data sources: CMAS, Walter & Presnall (1994), Gudfinnsson & Presnall (1996) and this study; CMAS–Na_2O, Walter & Presnall (1994); CMAS–'FeO', Gudfinnsson & Presnall (2000); CMAS–K_2O, this study.

porosity. This porosity would not be expected to survive at 1·1 GPa and 1310°C even in a subsolidus run (for example, a pure Fo charge would be expected to recrystallize to near 100% density in a few minutes at these conditions), and indeed it does not. However, the interesting observation is that the Fo layers are thoroughly impregnated with material that includes the components CaO and Al_2O_3 plus additional SiO_2, leading to the crystallization of Cpx, Opx and Sp among the original Fo. These components must come from the glass layer, through the action of a metastable melt present during the initial stages of the run. The metastable melt is inferred because the distances involved (~2 mm) are too large for solid state diffusion timescales. Whereas the initial olivine-only layers ended up with the assemblage Fo + Sp + Opx + Cpx, the glass layer crystallized to An + Sp + Opx + Cpx and is hence not in equilibrium with the Fo layers. No quenched melt was observed in the final run products (either Fo or glass starting layers), indicating that the run was, as expected, thoroughly subsolidus. We believe that the scenario whereby material migrates into the olivine layers may

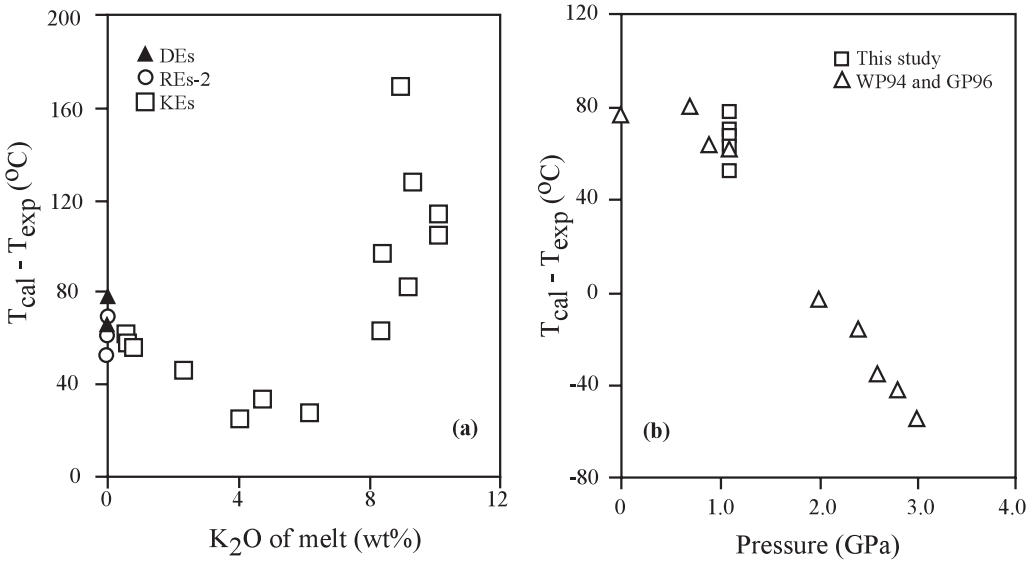

Fig. 15. The difference between temperatures calculated from the Ol/Melt MgO partitioning geothermometer of Ford *et al.* (1983) and the experimental temperature, plotted against (a) the K_2O content of the melt and (b) the experimental pressure. In (a) data are from this study in the systems CMAS and CMAS–K_2O, and in (b) data are from this study, WP94 (Walter & Presnall, 1994) and GP96 (Gudfinnsson & Presnall, 1996). The effect of pressure on thermocouple e.m.f. values is small compared with the observed discrepancies (e.g. see Figs 7 and 8) and cannot account for the pressure dependence of the temperature difference, implying that the geothermometer of Ford *et al.* (1983) needs to be further corrected for the effect of pressure.

be analogous to the processes occurring in diamond-aggregate melt-extraction experiments.

The diamond-aggregate technique was used to study the near-solidus partial melting of mantle peridotite (Johnson & Kushiro, 1992; Hirose & Kushiro, 1993; Baker & Stolper, 1994; Baker *et al.*, 1995; Kushiro, 1996). The results of one of these studies (Baker *et al.*, 1995) was questioned by Falloon *et al.* (1996), who drew attention to possible pitfalls in the technique, particularly when applied to experiments with low degrees of partial melting (where it is potentially most useful). Falloon *et al.* (1997, 1999) then checked some of the melt compositions observed in these studies and concluded that the diamond-aggregate technique compounds rather than solves the experimental problems. However, Kushiro (2001) has recently pointed out that 'the analyses given by Baker *et al.* (1995) were too low in alkalies because of wrong correction procedures (Hirschmann *et al.*, 1998)'. Kushiro therefore concluded that the results of Baker *et al.* were 'not inconsistent' with the tests of Falloon *et al.* (1997); but as Falloon *et al.* were evidently studying a different composition, consistency is difficult to judge. Although Kushiro (2001) inferred from this that 'The diamond aggregate method can be a reliable technique for obtaining and analyzing low-degree partial melt', we suggest that more testing is needed.

Full evaluation of the diamond-aggregate technique is beyond the scope of this study, but the observations obtained on C-1768 can be used to throw further doubt on the reliability of the diamond-aggregate technique at low melt fractions. The existence of the CaO, Al_2O_3 and extra SiO_2 amidst the Fo supports the argument of Falloon *et al.* (1996) that the initial intra-pore pressure can lead to metastable melt production. As another possible example of this, Hirose & Kushiro (1993) found melt in every single experiment of their diamond-aggregate study, despite several runs being at temperatures up to 50°C below the solidi of their two compositions as previously determined (Takahashi & Kushiro, 1983; Takahashi, 1986).

A defocused beam of approximately 40 μm × 50 μm was used to analyse areas in C-1768 from one end of the capsule to the other. The results are summarized in Fig. 18. Figure 18a shows that the amount of material infiltrating the Fo layers (as monitored by CaO and Al_2O_3) decreases away from the interface with the glass layer, but some still reaches the edge of the capsule. What is strange is the decrease in CaO/Al_2O_3 (Fig. 18b) from that in the initial glass ($CaO/Al_2O_3 = 0{\cdot}75$), which suggests decoupling of CaO and Al_2O_3. The transient melt in the Fo layers appears to have a much lower ratio than equilibrium melt coexisting with either Fo + Sp + Opx + Cpx or Sp + Opx + Cpx + An. A low CaO/Al_2O_3 ratio is also observed in many of the diamond-aggregate studies at low degrees of partial melting, although a true comparison is obscured by the high Na_2O contents of these melts. It would be valuable to test the diamond-aggregate method directly in the system CMAS at 1·1 GPa at subsolidus and near-solidus conditions. It is an accepted principle in the experimental

Table 6: CIPW norms of melts in the CMAS and CMAS–K_2O systems

	CMAS				CMAS−K_2O											
	KEs	P79	WP94	C-1565	C-1422	C-1461	C-1448	C-1460	C-1447	C-1574	C-1585	C-1779	C-1701	C-1708	C-1580	C-1576
T (°C):	1320	1350	1350	1320	1310	1310	1300	1290	1280	1270	1260	1250	1240	1230	1250	1230
Qz	0	0	0	0	0	0	0·51	0·84	2·88	6·09	1·86	1·56	4·94	3·44	13·72	20·83
Cor	0	0	0	0	0	0	0	0	0	0·35	0	1·35	0	0·25	2·32	2·58
Or	0	0	0	0	4·31	13·64	24·08	28·1	36·42	49·25	50·12	59·56	54·13	59·74	55·07	53·01
An	54·87	53·78	52·36	56·61	53·45	49·22	46·51	44·86	41·08	31·48	31·67	26·97	29·85	26·82	20·82	17·2
Di	16·49	17·88	16·78	15·82	14·77	11·38	7	5·35	2·49	0	1·63	0	0·71	0	0	0
Hy	23·43	22·61	23·99	26·81	24·36	23·98	21·8	20·75	17·03	12·7	14·62	10·47	10·56	9·67	8·01	6·32
Ol	5·14	5·68	7·01	0·66	3·03	1·69	0		0	0	0	0	0	0	0	0

KEs: regressed melt composition at $K_2O = 0$; P79, Presnall *et al.* (1979); WP94, Walter & Presnall (1994); the initial data are given in Table 5. We believe local equilibrium for the middle parts of C-1580 and C-1576 was achieved (see discussion in text). Qz, quartz; Cor, corundum; Or, orthoclase; An, anorthite; Di, diopside; Hy, hypersthene; Ol, olivine.

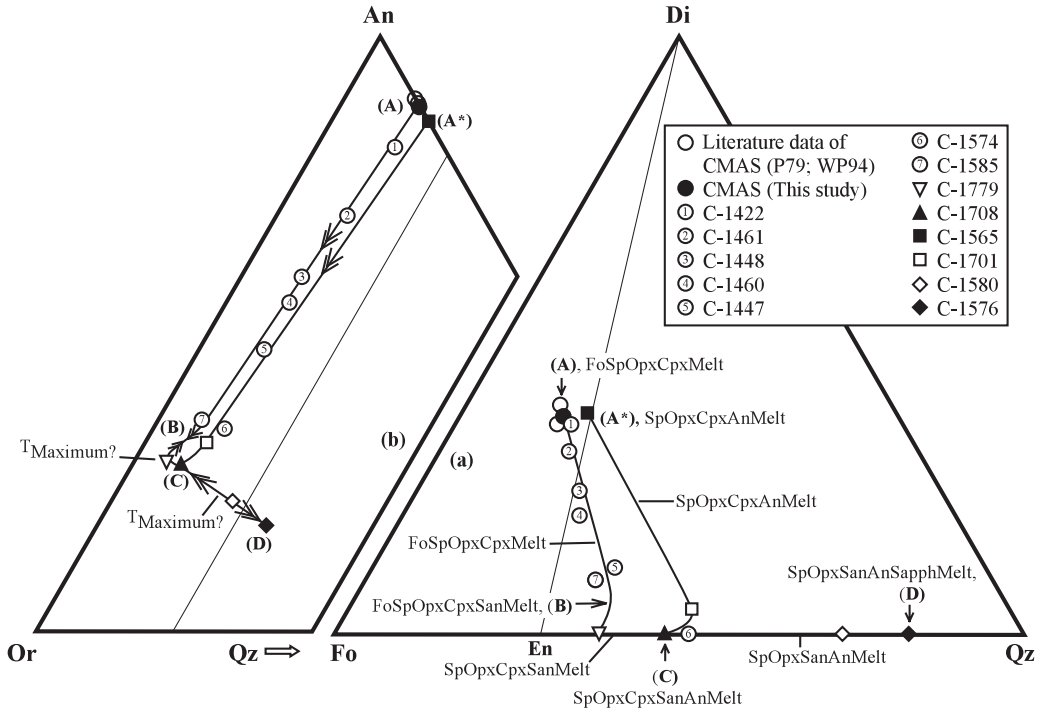

Fig. 16. Projections from An + Or (a) and from Fo + Di (b) showing the melt compositions in the KE experiments (wt %). CIPW norms are from Table 6. Projection (a) is inappropriate for melts with high K_2O content whereas (b) is inappropriate for melts with zero K_2O. In the former case, the melt compositions contain zero normative *ol* but high proportions of normative *an* and *or*, which do not appear in the projection; conversely, in the latter case, the melts are free of normative *or* but contain high amounts of normative *ol* and *di*. However, a combination of the two diagrams serves as an aid to visualizing the trends in melt composition. Points A and A* are the isobaric invariant points for Fo + Sp + Opx + Cpx + Melt and Sp + Opx + Cpx + An + Melt in the system CMAS, respectively. Points B, C and D, displaying six coexisting phases (Fo + Sp + Opx + Cpx + San + Melt, Sp + Opx + Cpx + San + An + Melt and Sp + Opx + San + An + Sapph + Melt), are the isobaric invariant points in the system CMAS–K_2O. Temperature fall shown by arrows is based on direct experimental observation or on calculation using the phase composition data at the invariant points B, C or D with the method of Presnall (1986). Between point B and point C, and point C and point D, there are two temperature maxima. Their position has not been located directly. The partial melting reactions in this portion of the system CMAS–K_2O are all peritectic.

petrology of subsolidus phase equilibria that the attainment of equilibrium should be tested by performing reversal experiments; this principle would seem to equally important in the case of melt-extraction experiments, which could be tested very effectively using the kind of reversals presented in this study.

The anorthite–sanidine solvus

Anorthite, albite (Ab) and sanidine are the three main components of natural feldspars. At high temperatures there is complete solid solution across the joins An–Ab (plagioclase) and Ab–San (alkali feldspar), but the solvus between An and San extends to their solidus. Despite the usefulness of the An–San solvus for constraining thermodynamic models of ternary feldspar solid solutions (Nekvasil, 1994), there are only two experimental studies on the binary An–San join at high temperatures (Ai & Green, 1989; Nekvasil & Carroll, 1993), which disagree on the compositions of the coexisting feldspars as well as on the temperature of the solidus. Ai & Green (1989) located the eutectic in the An–San binary at 1·0 GPa at $An_{30}San_{70}$ and 1215 ± 15°C, and found the maximum mutual solubility of 18% San in An (by mole) and 7% An in San (Fig. 19). Nekvasil & Carroll (1993), however, found the eutectic at 1·13 GPa at $An_{19}San_{81}$ and 1280 ± 10°C, and the maximum mutual solubility is 11% San in An and 9% An in San (Fig. 19).

Determining the phase relations around the An–San solvus and solidus is experimentally more difficult than it may seem at first sight. The kinetics of the mixing/unmixing process at the solvus are too sluggish for direct experimental investigation at subsolidus conditions. The assemblage An_{ss} + San_{ss} + Melt is isobarically invariant in the system $CaAl_2Si_2O_8$–$KAlSi_3O_8$, and thus observing this assemblage directly is not theoretically possible in the pure system (this is of course exactly the same problem we confront in this study). Indeed, the reported observations of both the Ai & Green (1989) and Nekvasil & Carroll (1993) on the solvus/solidus relations are inferences obtained by the bracketing technique.

In the same way that adding K_2O to the system CMAS enables us to constrain the phase relations around

Table 7: Regression coefficients for phases of variable compositions in experiments with Fo + Sp + Opx + Cpx + Melt

		CaO	MgO	Al_2O_3	SiO_2	K_2O
Melt	A	0·0016925	0·0019498	−0·0006571	−0·0015076	−0·0014776
	B	−4·206728	−4·848343	1·678342	3·718272	3·658458
	C	2620·00	3018·51	−1050·26	−2233·04	−2255·22
	D	0·64	0·70	0·34	0·82	0·54
Cpx	A	−0·0000256	−0·0001765	0·0008478	−0·0006457	—
	B	0·055271	0·460585	−2·177688	1·661832	—
	C	−10·17	−279·40	1406·49	−1016·92	—
	D	0·16	0·15	0·22	0·09	—
Opx	A	−0·0000508	−0·0002918	0·0005426	−0·0002001	—
	B	0·138646	0·742252	−1·392491	0·511593	—
	C	−92·14	−437·08	901·53	−272·31	—
	D	0·12	0·14	0·15	0·12	—

Regression equation is $X_i^\phi = AT^2 + BT + C$, where X_i^ϕ is the concentration in weight percent of oxide i in phase ϕ and T is in °C. D is the average difference between regressed and experimentally observed values.

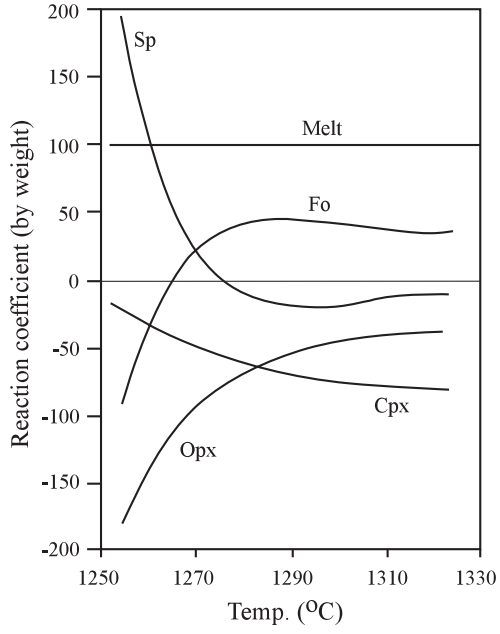

Fig. 17. The melting reaction along the univariant curve of Sp-lherzolite in system CMAS–K_2O (from point A to point B in Fig. 16): reaction coefficients (n_i) for the reaction $0 = n_{ol}$ Ol + n_{opx} Opx + n_{cpx} Cpx + n Sp + 100 Melt. Rising temperature corresponds to decreasing K_2O content of the melt. The method of calculating the coefficients of the melting reaction is from Walter *et al.* (1995). The melting reaction is independent of the bulk composition as long as all the phases coexist.

the Fo + Opx + Cpx + Sp + Melt invariant point, so the presence of MgO plus other minor CAS components in our experiments increases the variance of the system and enables us to observe An_{ss} + San_{ss} + Melt directly. We are thus able to report some useful points on the solvus, and also to put some constraints on the solidus of the $CaAl_2Si_2O_8$–$KAlSi_3O_8$ system at 1·1 GPa.

We have three runs that produced coexisting An_{ss} and San_{ss} (C-1580 at 1250°C and C-1708 and C-1576 at 1230°C), which are shown projected onto the $CaAl_2Si_2O_8$–$KAlSi_3O_8$ join in Fig. 19. The maximum mutual solubility of An and San observed here is higher than that of Ai & Green (1989) and much higher than that of Nekvasil & Carroll (1993). These new data suggest that the feldspar model calibrated by Fuhrman & Lindsley (1988) has the best performance at higher temperatures. As shown by Nekvasil (1994), all other models calculate much lower mutual solubilities of An and San.

Because MgO concentrates in the melt relative to An_{ss} and San_{ss}, the eutectic in the MgO-free system $CaAl_2Si_2O_8$–$KAlSi_3O_8$ at 1·1 GPa must be higher than 1250°C (run C-1580). Allowing for a representative slope dT/dP for silicate melting of about 100°C/GPa, our results are not consistent with the solidus temperature of 1215 ± 15°C at 1·0 GPa found by Ai & Green (1989), but are consistent with the 1280 ± 10°C at 1·13 GPa suggested by Nekvasil & Carroll (1993). The molar Ca/(Ca + K) ratios in our three melts in equilibrium with An + San are 0·31, 0·27 and 0·25. On the grounds that some of the Ca in the melt is presumably associated with components other than An, but all the K can be assigned to a San component, we surmise that the composition of the solidus (eutectic) melt in the binary $CaAl_2Si_2O_8$–$KAlSi_3O_8$ would lie at lower molar Ca/(Ca + K), again

Table 8: Comparison of melting reactions in the CMAS, CMAS–Na_2O and CMAS–K_2O systems at 1·1 GPa

System	*T* (°C)	Method*	Reaction (wt %)	Reference†
CMAS	1350	Korzhinskii	46·8 Opx + 71·4 Cpx + 11·7 Sp = 100·0 Melt + 29·9 Fo	GP96
CMAS	1320	Korzhinskii	40·7 Opx + 79·7 Cpx + 13·8 Sp = 100·0 Melt + 34·2 Fo	This study
CMAS	~1320	Korzhinskii	26·2 Opx + 26·2 Cpx + 50·1 An = 100·0 Melt + 2·5 Sp	This study
CMASN	—	Walter95	46 Opx + 75 Cpx + 13 Sp = 100 Melt + 34 Fo	Walter95
CMASK	1310	Walter95	41·5 Opx + 79·1 Cpx + 15·1 Sp = 100·0 Melt + 35·7 Fo	This study
CMASK	1280	Walter95	69·5 Opx + 58·9 Cpx + 9·4 Sp = 100·0 Melt + 37·8 Fo	This study
CMASK	1270	Walter95	94·8 Opx + 47·9 Cpx = 100·0 Melt + 17·4 Fo + 25·3 Sp	This study
CMASK	1260	Walter95	140·7 Opx + 33·0 Cpx + 36·4 Fo = 100·0 Melt + 110·1 Sp	This study
CMASK	1255	Walter95	181·5 Opx + 21·8 Cpx + 91·0 Fo = 100·0 Melt + 194·2 Sp	This study
CMASK	1252?	Korzhinskii	5·4 Sp + 20·7 Opx + 15·4 Cpx + 71·7 San = 100·0 Melt + 13·2 Fo	This study
CMASK	1230	Korzhinskii	23·4 An + 66·5 San + 12·7 Opx = 100·0 Melt + 1·7 Sp + 0·9 Cpx	This study
CMASK	1230	Korzhinskii	9·6 An + 63·0 San + 122·2 Sapph. = 100·0 Melt + 89·9 Sp + 4·8 Px	This study

*Method: Korzhinskii, Korzhinskii (1959); Walter95, Walter *et al.* (1995).
†References: GP96, Gudfinnsson & Presnall (1996); Walter95, Walter *et al.* (1995).
To calculate the reaction for the isobaric invariant point Fo + Sp + Opx + Cpx + San + Melt at ~1252°C, Fo was added to the phase assemblage observed in C-1779.

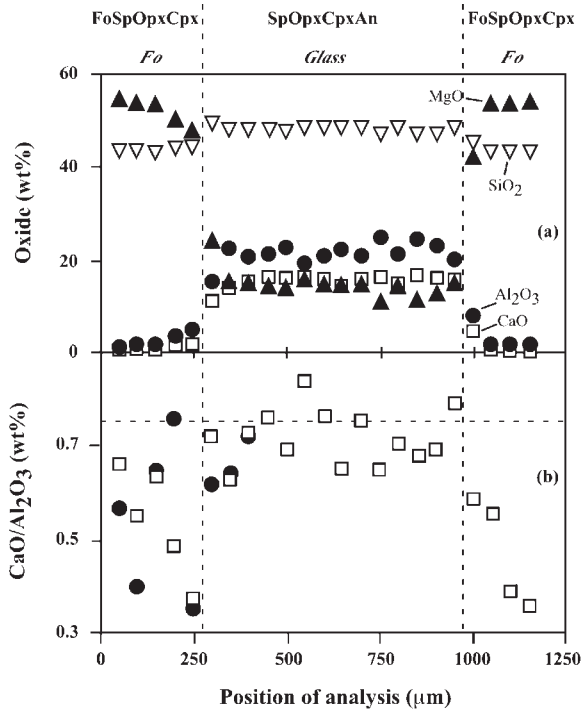

Fig. 18. Variation in composition along the sectioned capsule from experiment C-1768, a sandwich experiment in which the starting geometry consisted of a layer of glass placed between two layers of pure Fo. Despite being completely subsolidus, a component containing CaO and Al_2O_3 has infiltrated into the Fo layers. Analyses were obtained using a defocused beam (~40 μm × 50 μm). (a) shows a complete profile from one end of the capsule to the other; (b) shows this complete profile (□) and also another incomplete profile (●), extending to the glass layer.

consistent with the phase diagram of Nekvasil & Carroll (1993) (eutectic at $An_{19}San_{81}$), rather than that of Ai & Green (1989) ($An_{30}San_{70}$).

Sapphirine

In two of the sandwich experiments (C-1580 and C-1576), the middle melt-rich regions produced an assemblage containing sapphirine (Sapph); the phase assemblage consisted of An + San + Sapph + Melt at 1250°C (C-1580), which was joined by Opx and Sp at 1230°C to form the isobarically invariant assemblage An + San + Sapph + Sp + Opx + Melt. Neither assemblage is in equilibrium with the end regions, which consisted of the usual Fo + Opx + Cpx + Sp with no apparent melt, and with a texture showing minimal recrystallization, also indicative of no melt. However, the compositions of the pyroxenes in these regions are consistent with local equilibrium. Sapph is incompatible with Fo at 1·1 GPa and ~1250°C, reacting to form Opx + Sp (e.g. Liu & Presnall, 2000). A semi-schematic phase diagram showing the subsolidus phase relations in the system MgO–Al_2O_3–SiO_2 at ~1250°C and 1·1 GPa is shown in Fig. 20.

In C-1576, the Opx in the two regions was very different in composition; that in the subsolidus peridotitic assemblage had the usual 8·5 wt % Al_2O_3 (consistent with other experiments), whereas that in the sapphirine-bearing middle region had 14 wt %. The regions are separated by a thin band of orthopyroxene ~10 μm in width (Fig. 2a). Remarkably, the composition of the orthopyroxene changes across this narrow band, from

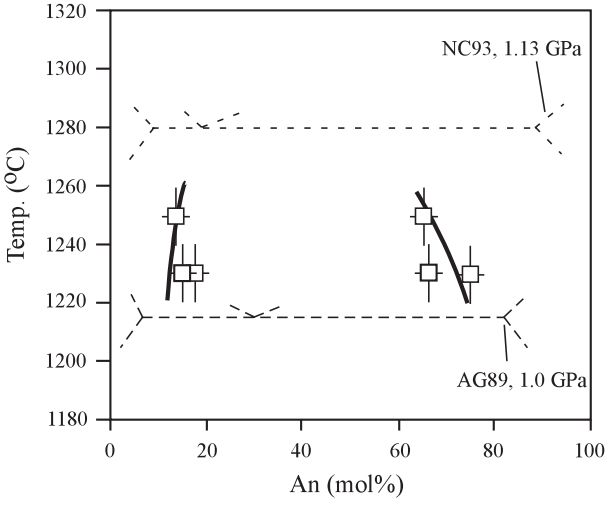

Fig. 19. The mutual solubility (mol %) of San and An at 1·1 GPa. Also plotted are the experimentally determined phase relations in the system $CaAl_2Si_2O_8$–$KAlSi_3O_8$ from Ai & Green (1989) at 1·0 GPa (AG89), and from Nekvasil & Carroll (1993) at 1·13 GPa (NC93). The small amounts of MgO, up to ~0·6 wt %, found in An in this study have been ignored. As discussed in the text, our (unreversed) data support the results of Nekvasil & Carroll (1993) as regards temperature, but indicate higher mutual solubilities, the compositional difference being most marked for the An-rich limb of the solvus.

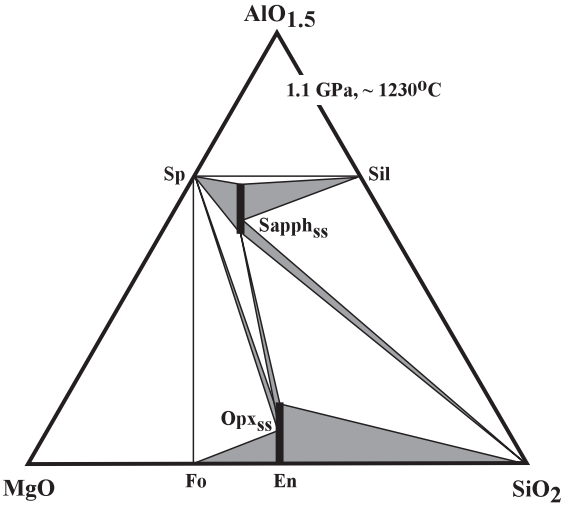

Fig. 20. Subsolidus phase relationships in the system MgO–$AlO_{1·5}$–SiO_2 at 1·1 GPa and ~1230°C. Small amounts of CaO in Opx, Fo and possibly other phases are ignored. The shaded areas are two-phase fields resulting from the compositional variability of Opx and Sapph.

the 14 wt % of the An + San + Sapph + Sp + Opx + Melt assemblage on that side, to the 8·5 wt % on the other (see Fig. 2a).

The solubility of Al_2O_3 in Opx in equilibrium with Sapph + Qz (quartz) has recently been studied by Hollis & Harley (2002) at P–T conditions close to those of this study. The controlling reaction can be written

$$4\ MgAl_2SiO_6 = Mg_4Al_4Si_2O_{20} + 2\ SiO_2. \quad (8)$$
$$\text{Opx} \qquad \text{Sapph}$$

Thus lowering the activity of SiO_2 should move equilibrium (8) towards the right-hand side, lowering Al_2O_3 in Opx (see also Fig. 20). However, the Al_2O_3 content of the Opx in equilibrium with Sapph + Sp in our experiment C-1576 is significantly higher than found by Hollis & Harley (2002) at similar temperatures and pressures (e.g. their experiments R50a,b at 1250°C and 1·2 GPa have only 9·5–10·5 wt % Al_2O_3 in Opx). Our experiment, unlike those of Hollis & Harley (2002), is unreversed, so that it is possible that we are observing metastable Opx, rapidly crystallized from melt at the start of the experiment. However, the Opx and Sapph in this experiment are both homogeneous and euhedral (Fig. 2a).

The compositional variation of sapphirine in the MgO–Al_2O_3–SiO_2 system can be considered by starting with the basic formula $Mg_4Al_4Si_2O_{20}$ (called 2:2:1 sapphirine). Most natural sapphirines are more aluminous than this, as a result of substitution of 2Al for Mg + Si (i.e. solid solution towards the 7:9:3 composition, $Mg_7Al_9Si_3O_{20}$; e.g. Liu & Presnall, 2000; Hollis & Harley, 2002); here, by contrast, the reverse substitution of Mg + Si for 2Al occurs, to produce sapphirines with less alumina than in 2:2:1, as found by Liu & Presnall (2000). Thus if the formula is represented as $Mg_{4-x}Al_{4+2x}Si_{2-x}O_{20}$, x is usually in the range 0–0·5 (Hollis & Harley, 2002), but here x is approximately −0·15 in C-1580 and −0·3 in C-1576. Figure 20 confirms that $Sapph_{ss}$ in equilibrium with Opx should contain the minimum Al_2O_3 at a given P and T.

CONCLUSIONS

In this study, we made forward partial melting experiments to determine the phase relations at the solidus of the spinel-lherzolite assemblage in the system CMAS both with and without K_2O. We also made reversal crystallization experiments. The K_2O method, thus, can be fully assessed both by internal consistency and by reference to the previous literature data (Presnall, 1976; Presnall *et al.*, 1979; Walter & Presnall, 1994).

Compositions of all phases, including both pyroxene solid solutions and the melt compositions in the system CMAS derived from the KEs by extrapolating to zero K_2O, agree reasonably well with previous studies. The melt composition of Presnall *et al.* (1979) is almost the same as our extrapolated result from the KEs.

Agreement on the solidus temperature for a Sp-lherzolite phase assemblage in the system CMAS at 1·1 GPa is consistent between the KEs and the REs and it is around 1320°C, with a probable uncertainty of less than ±10°C.

The slightly higher temperature of 1350°C determined by Presnall (1976), later used in Presnall *et al.* (1979), Walter & Presnall (1994) and Gudfinnsson & Presnall (1996, 2000, 2001), may be due to the W/Re thermocouples used in that study, either from oxidation or from calibration errors. The oxidation problem of the W/Re thermocouples forced Walter & Presnall (1994) to use a nitrogen flow down the thermocouple insulator for their experiments at lower pressures. Recently, Falloon *et al.* (2001) reported drift of W/Re thermocouples at 1·0 GPa to higher apparent temperature in the temperature range 1300–1400°C caused by oxidation. Commercially available W/Re thermocouples vary widely in their deviation from theoretical e.m.f.–temperature relations, requiring careful calibration of each batch (see Klemme & O'Neill, 2000*b*).

The obvious agreement on the pyroxene composition, the melt composition and the solidus among the extrapolation result from the KEs, the result of the REs and the literature data argues that the K_2O method is generally successful. We will report on the application of this method to the determination of partial melting at the solidus in the system CMAS–Cr_2O_3 in another paper (Liu & O'Neill, in preparation).

Comparison with previous work on the system CMAS–Na_2O shows that the effect of K_2O on melting equilibria is much stronger than that of Na_2O, both as regards temperature and melt composition. Increasing K_2O causes the multiply-saturated solidus melt composition to trend towards silica enrichment, becoming quartz-normative above 4 wt % K_2O. By contrast, the effect of Na_2O at 1·1 GPa is for multiply-saturated melts to trend towards becoming more silica undersaturated; high Na_2O melts are *ne*-normative (where *ne* is nepheline). It should be noted, however, that the activity of SiO_2 in both systems remains nearly the same, being buffered by Fo + Opx [reaction (3)].

ACKNOWLEDGEMENTS

We acknowledge the technical assistance of Bill Hibberson, Dean Scott, Nick Ware, Mike Shelley, Harry Kokkonen, Frank Brink, and Drs Roger Heady, Cheng Huang, Sue Kesson and Uli Troitzsch. Ruby discs were supplied by Dr John Mavrogenes. We benefited from constructive discussions with Professor David Green and Drs Jorg Hemann and Sue Kesson. This study is part of the Ph.D. thesis of L.X. funded by A. E. Ringwood Memorial Scholarship and Australian International Postgraduate Research Scholarship. L.X. also thanks Dr Shen-su Sun and Professor Qingchen Wang for their encouragement. We thank Leonid Danyushevsky and Richard Arculus for their reviews, and the latter for his editorial handling.

REFERENCES

Ai, Y. & Green, D. H. (1989). Phase relations in the system anorthite–potassium feldspar at 10 kbar with emphasis on their solid solutions. *Mineralogical Magazine* **53**, 337–345.

Baker, M. B. & Stolper, E. M. (1994). Determining the composition of high-pressure mantle melts using diamond aggregates. *Geochimica et Cosmochimica Acta* **58**, 2811–2827.

Baker, M. B., Newman, S., Beckett, J. R. & Stolper, E. M. (1992). Separating liquid from crystals in high-pressure melting experiments using diamond aggregates. *Geological Society of America, Programs with Abstracts* **24**, A256.

Baker, M. B., Hirschmann, M. M., Ghiorso, M. S. & Stolper, E. M. (1995). Compositions of near-solidus peridotite melts from experiments and thermodynamics calculation. *Nature* **375**, 308–311.

Baker, M. B., Hirschmann, M. M., Wasylenki, L. E. & Stolper, E. M. (1996). Quest for low-degree mantle melts: a reply. *Nature* **381**, 285.

Bose, K. & Ganguly, J. (1995). Quartz–coesite transition revisited: reversed experimental determination at 500–1200°C and retrieved thermochemical properties. *American Mineralogist* **80**, 231–238.

Boyd, F. R. & England, J. L. (1960). Apparatus for phase-equilibrium measurements at pressures up to 50 kbar and temperatures up to 1750°C. *Journal of Geophysical Research* **65**, 741–748.

Brey, G. P. & Kohler, T. (1990). Geothermobarometry in four-phase lherzolite II: new thermobarometers, and practical assessment of existing thermobarometers. *Journal of Petrology* **31**, 1353–1378.

Chen, C.-H. & Presnall, D. C. (1975). The system Mg_2SiO_4–SiO_2 at pressures up to 25 kilobars. *American Mineralogist* **60**, 398–406.

Danckwerth, P. A. & Newton, R. C. (1978). Experimental determination of the spinel peridotite to garnet peridotite reaction in the system MgO–Al_2O_3–SiO_2 in the range 900°–1100°C and Al_2O_3 isopleths of enstatite in the spinel field. *Contributions to Mineralogy and Petrology* **66**, 189–201.

Danyushevsky, L. V., Sololev, A. V. & Dmitriev, L. V. (1996). Estimation of the pressure of crystallisation and H_2O content of MORB and BABB glasses: calibration of an empirical technique. *Mineralogy and Petrology* **57**, 185–204.

Falloon, T. J. & Danyushevsky, L. V. (2000). Melting of refractory mantle at 1·5, 2 and 2·5 GPa under anhydrous and H_2O-undersaturated conditions: implications for the petrogenesis of high-Ca boninites and the influences of subduction components on mantle melting. *Journal of Petrology* **41**, 257–283.

Falloon, T. J. & Green, D. H. (1987). Anhydrous partial melting of MORB pyrolite and other peridotite compositions at 10 kbar: implications for the origin of MORB glasses. *Mineralogy and Petrology* **37**, 181–219.

Falloon, T. J. & Green, D. H. (1988). Anhydrous partial melting of peridotite from 8 to 35 kbars and the petrogenesis of MORB. *Journal of Petrology, Special Issue* 379–414.

Falloon, T. J., Green, D. H., O'Neill, H. St. C. & Ballhaus, C. G. (1996). Quest for low-degree mantle melts. *Nature* **381**, 285.

Falloon, T. J., Green, D. H., O'Neill, H. St. C. & Hibberson, W. O. (1997). Experimental tests of low degree peridotite partial melt compositions: implications for the nature of anhydrous near-solidus peridotite melts at 1 GPa. *Earth and Planetary Science Letters* **152**, 149–162.

Falloon, T. J., Green, D. H., Danyushevsky, L. V. & Faul, U. H. (1999). Peridotite melting at 1·0 and 1·5 GPa: an experimental evaluation of techniques using diamond aggregates and mineral mixes for determination of near-solidus melts. *Journal of Petrology* **40**, 1343–1375.

Falloon, T. J., Danyushevsky, L. V. & Green, D. H. (2001). Peridotite melting at 1 GPa: reversal experiments on partial melt compositions

produced by peridotite–basalt sandwich experiments. *Journal of Petrology* **42**, 2363–2390.

Ford, C. E., Russell, D. G., Graven, J. A. & Fisk, M. R. (1983). Olivine–liquid equilibria: temperature, pressure and composition dependence of the crystal/liquid cation partition coefficients for Mg, Fe^{2+}, Ca and Mn. *Journal of Petrology* **24**, 256–265.

Fuhrman, M. L. & Lindsley, D. H. (1988). Ternary-feldspar modelling and thermometry. *American Mineralogist* **75**, 544–559.

Fujii, T. (1977). Pyroxene equilibria in spinel lherzolite. *Carnegie Institution of Washington Yearbook* **76**, 569–572.

Fujii, T. & Scarfe, C. M. (1985). Composition of liquids coexisting with spinel lherzolite at 10 kbar and the genesis of MORBs. *Contributions to Mineralogy and Petrology* **131**, 323–346.

Gasparik, T. (1984). Two-pyroxene thermobarometry with new experiment data in the system CaO–MgO–Al_2O_3–SiO_2. *Contributions to Mineralogy and Petrology* **87**, 87–97.

Green, T. H., Ringwood, A. E. & Major, A. (1966). Friction effects and pressure calibration in a piston-cylinder high pressure–temperature apparatus. *Journal of Geophysical Research* **71**, 3589–3594.

Gudfinnsson, G. H. & Presnall, D. C. (1996). Melting relations of model lherzolite in the system CaO–MgO–Al_2O_3–SiO_2 at 2·4–3·4 GPa and the generation of komatiites. *Journal of Geophysical Research* **101**, 27701–27709.

Gudfinnsson, G. H. & Presnall, D. C. (2000). Melting behaviour of model lherzolite in the system CaO–MgO–Al_2O_3–SiO_2–FeO at 0·7–2·8 GPa. *Journal of Petrology* **41**, 1241–1269.

Gudfinnsson, G. H. & Presnall, D. C. (2001). A pressure-independent geothermometer for primitive mantle melts. *Journal of Geophysical Research* **106**, 16205–16211.

Herzberg, C. (1978). Pyroxene geothermometry and geobarometry: experimental and thermodynamic evaluation of some subsolidus phase relations involving pyroxenes in the system CaO–MgO–Al_2O_3–SiO_2. *Geochimica et Cosmochimica Acta* **42**, 945–957.

Herzberg, C. & Zhang, J. (1998). Melting experiments in the systems CaO–MgO–Al_2O_3–SiO_2 and MgO–SiO_2 at 3 to 15 GPa. *American Mineralogist* **83**, 491–500.

Hirose, K. (1997). Melting experiments on lherzolite KLB-1 under hydrous conditions and generation of high-magnesian andesitic melts. *Geology* **25**, 42–44.

Hirose, K. & Kawamoto, T. (1995). Hydrous partial melting of lherzolite at 1 GPa: the effect of H_2O on the genesis of basaltic magmas. *Earth and Planetary Science Letters* **133**, 463–473.

Hirose, K. & Kushiro, I. (1993). Partial melting of dry peridotite at high pressures: determination of compositions of melts segregated from peridotite using aggregates of diamond. *Earth and Planetary Science Letters* **114**, 477–489.

Hirschmann, M. M., Baker, M. B. & Stolper, E. M. (1998). The effect of alkalis on the silica content of mantle-derived magmas. *Geochimica et Cosmochimica Acta* **62**(5), 883–902.

Hollis, J. A. & Harley, S. L. (2002). Alumina solubility in orthopyroxene coexisting with sapphirine and quartz. *Contributions to Mineralogy and Petrology* DOI 10.1007/s00410-002-0412-3.

Jochum, K. P., Dingwell, D. B., Rocholl, A., *et al.* (2000). The preparation and preliminary characterisation of eight geological MPI-DING reference glasses for in-situ microanalysis. *Journal of Geostandards and Geoanalysis* **24**, 87–133.

Johannes, W., Bell, P. M., Mao, H. K., Boettcher, A. L., Chipman, D. W., Hays, J. F., Newton, R. C. & Seifert, F. (1971). An interlaboratory comparison of piston-cylinder pressure calibration using albite-breakdown reaction. *Contributions to Mineralogy and Petrology* **32**, 24–38.

Johnson, K. T. M. & Kushiro, I. (1992). Segregation of high pressure partial melts from peridotite using aggregates of diamond: a new experimental approach. *Geophysical Research Letters* **19**, 1703–1706.

Klemme, S. & O'Neill, H. St. C. (1997). The reaction $MgCr_2O_4$ + SiO_2 = Cr_2O_3 + $MgSiO_3$ and the free energy of formation of magnesiochromite ($MgCr_2O_4$). *Contributions to Mineralogy and Petrology* **130**, 59–65.

Klemme, S. & O'Neill, H. St. C. (2000*a*). The near-solidus transition from garnet lherzolite to spinel lherzolite. *Contributions to Mineralogy and Petrology* **138**, 237–248.

Klemme, S. & O'Neill, H. St. C. (2000*b*). The effect of Cr on the solubility of Al in orthopyroxene: experiments and thermodynamic modelling. *Contributions to Mineralogy and Petrology* **140**, 84–98.

Korzhinskii, D. S. (1959). *Physicochemical Basis of the Analysis of the Paragenesis of Minerals*. New York: Consultants Bureau.

Kushiro, I. (1972). Partial melting of synthetic and natural peridotites at high pressures. *Carnegie Institution of Washington Yearbook* **71**, 357–362.

Kushiro, I. (1996). Partial melting of a fertile mantle peridotite at high pressure: an experimental study using aggregates of diamond. In: Basu, A. & Hart, S. R. (eds) *Earth Processes: Reading the Isotopic Code. American Geophysical Union, Geophysical Monograph* **95**, 109–122.

Kushiro, I. (2001). Partial melting experiments on peridotite and origin of mid-ocean ridge basalt. *Annual Review of Earth and Planetary Sciences* **29**, 71–107.

Kushiro, I. & Hirose, K. (1992). Experimental determination of composition of melt formed by equilibrium partial melting of peridotite at high pressures using aggregates of diamond grains. *Proceedings of the Japanese Academy, Series B* **68**, 63–68.

Lane, D. L. & Ganguly, J. (1980). Al_2O_3 solubility in orthopyroxene in the system MgO–Al_2O_3–SiO_2: a re-evaluation, and mantle geotherm. *Journal of Geophysical Research* **85**, 6963–6972.

Leeman, W. P. (1978). Distribution of Mg^{2+} between olivine and silicate melt, and its implications regarding melt structure. *Geochimica et Cosmochimica Acta* **42**, 789–800.

Liu, T. C. & Presnall, D. C. (1990). Liquidus phase relationships on the join anorthite–forsterite–quartz at 20 kbar with applications to basalt petrogenesis and igneous sapphirine. *Contributions to Mineralogy and Petrology* **104**, 735–742.

Liu, T. C. & Presnall, D. C. (2000). Liquidus phase relations in the system CaO–MgO–Al_2O_3–SiO_2 at 2·0 GPa: applications to basalt fractionation, eclogites, and igneous sapphirine. *Journal of Petrology* **41**, 3–20.

Longhi, J. (1987). Liquidus equilibrium and solid solution in the system $CaAl_2Si_2O_8$–$CaSiO_3$–SiO_2 at low pressure. *American Journal of Science* **287**, 265–331.

Milholland, C. S. & Presnall, D. C. (1998). Liquidus phase relations in the CaO–MgO–Al_2O_3–SiO_2 system at 3·0 GPa; the aluminous pyroxene thermal divide and high-pressure fraction of picritic and komatiitic magmas. *Journal of Petrology* **39**, 3–27.

Nekvasil, H. (1994). Ternary feldspar/melt equilibria: a review. In: Parson, I. (ed.) *Feldspars and their Reactions. NATO ASI Series C* **421**, 195–219.

Nekvasil, H. & Carroll, W. (1993). Experimental constraints on the high-temperature termination of the anhydrous 2 feldspar + L curve in the feldspar system at 11·3 kbar. *American Mineralogist* **78**, 601–606.

Nickel, K. G., Brey, G. P. & Kogarto, L. (1985). Orthopyroxene–clinopyroxene equilibria in the system CaO–MgO–Al_2O_3–SiO_2. *Contributions to Mineralogy and Petrology* **91**, 44–53.

Obata, M. (1976). The solubility of Al_2O_3 in orthopyroxenes in spinel and plagioclase peridotites and spinel pyroxenite. *American Mineralogist* **61**, 804–816.

O'Hara, M. J. (1968). The bearing of phase equilibria studies in synthetic and natural systems on the origin and evolution of basic and ultrabasic rocks. *Earth-Science Reviews* **4**, 69–133.

O'Neill, H. St. C. & Eggins, S. M. (2002). The effect of melt composition on trace element partitioning: an experimental investigation of the activity coefficients of FeO, NiO, CoO, MoO_2 and MoO_3 in silicate melts. *Chemical Geology* **186**, 151–181.

Presnall, D. C. (1976). Alumina content of enstatite as a geobarometer for plagioclase and Sp-lherzolites. *American Mineralogist* **61**, 582–588.

Presnall, D. C. (1986). An algebraic method for determining equilibrium crystallization and fusion paths in multicomponent systems. *American Mineralogist* **71**, 1061–1070.

Presnall, D. C. (1999). Effect of pressure on the fractional crystallisation of basaltic magma. In: Fei, Y., Bertka, C. M. & Mysen, B. O. (eds) *Mantle Petrology: Field Observations and High Pressure Experimentation: a Tribute to Francis R. (Joe) Boyd. Geochemical Society, Special Publication* **6**, 209–224.

Presnall, D. C., Dixon, S. A., Dixon, J. R., O'Donnell, T. H., Brenner, N. L., Schrock, R. L. & Dycus, D. W. (1978). Liquidus phase relations on the joint diopside–forsterite–anorthite from 1 atm. to 20 kbar: their bearing on the generation and crystallization of basaltic magma. *Contributions to Mineralogy and Petrology* **66**, 203–220.

Presnall, D. C., Dixon, J. R., O'Donnell, T. H. & Dixon, S. A. (1979). Generation of mid-ocean ridge tholeiites. *Journal of Petrology* **20**, 3–36.

Robinson, J. A. C., Wood, B. J. & Blundy, J. D. (1998). The beginning of melting of fertile and depleted peridotite at 1·5 GPa. *Earth and Planetary Science Letters* **155**, 97–111.

Sen, G. (1985). Experimental determination of pyroxene compositions in the system $CaO–MgO–Al_2O_3–SiO_2$ at 900–1200°C and 10–15 kbar using PbO and H_2O fluxes. *American Mineralogist* **70**, 678–695.

Sen, G. & Presnall, D. C. (1984). Liquidus phase relationships on the join anorthite–forsterite–quartz at 10 bar with applications to basalt petrogenesis. *Contributions to Mineralogy and Petrology* **85**, 404–408.

Stolper, E. (1980). A phase diagram for mid-ocean ridge basalts: preliminary results and implications for petrogenesis. *Contributions to Mineralogy and Petrology* **74**, 13–27.

Takahashi, E. (1986). Melting of a dry peridotite KLB-1 up to 14 GPa: implications on the origin of peridotitic upper mantle. *Journal of Geophysical Research* **91**, 9367–9382.

Takahashi, E. & Kushiro, I. (1983). Melting of a dry peridotite at high pressures and basalt magma genesis. *American Mineralogist* **68**, 859–879.

Walter, M. J. & Presnall, D. C. (1994). Melting behaviour of simplified lherzolite in the system $CaO–MgO–Al_2O_3–Na_2O$ from 7 to 35 kbar. *Journal of Petrology* **35**, 329–359.

Walter, M. J., Sisson, T. W. & Presnall, D. C. (1995). A mass proportion method for calculating melting reaction and application to melting of model upper mantle lherzolite. *Earth and Planetary Science Letters* **135**, 77–90.

Ware, N. G. (1991). Combined energy-dispersive–wavelength-dispersive quantitative electron microprobe analysis. *X-Ray Spectrometry* **20**, 73–79.